The technical, economic, and environmental feasibility of a bioheat-driven adsorption cooling system for food cold storing: A case study of Rwanda

Ahmed A Alammar[1,2], Ahmed Rezk[*2,3], Abed Alaswad[2,3], Julia Fernando[4], A. G. Olabi[*3,5], Stephanie Decker[7], Joseph Ruhumuliza[7], Quénan Gasana[7]

[1]Center for Sustainable Cooling, School of Chemical Engineering, University of Birmingham, Birmingham, B15 2TT

[2]Energy and Bioproducts Research Institute (EBRI), College of Engineering and Physical Science, Aston University, Birmingham, UK, B4 7ET

[3]Mechanical, Biomedical and Design, College of Engineering and Physical Science, Aston University, Birmingham, UK, B4 7ET

[4]Aston Business School, Aston University, Birmingham, UK, B4 7ET

[5]Sustainable and Renewable Energy Engineering Department, University of Sharjah, United Arab Emirates

[6]School of Management, University of Bristol, UK, BS8 1TH

[7]Department of Agricultural Mechanization, School of Agricultural Engineering, University of Rwanda, Rwanda

Abstract

This paper studies the technical, economic, and environmental feasibility of a standalone adsorption cooling system thermally driven by biomass combustion and solar thermal energy. The developed cooling package was benchmarked against a baseline vapour compression refrigeration system, driven by grid electricity and the widely investigated adsorption cooling system driven by solar heat. TRNSYS was utilised to imitate the integrated systems, investigate their performance throughout the year, and optimise their designs by employing the meteorological data for Rwanda and an existing cold room (13 m^2 floor area × 2.9 m height) as a case study. The optimisation study for the system revealed that maximum chiller performance (COP = 0.62), minimum biomass daily consumption (36 kg), and desired cold room setting temperature (10 °C) throughout the year can be achieved if the boiler setting temperature, heat storage size, and heating water flow rate are 95.13 °C, 0.01 m^3 and 601.25 Kg/h. An optimal PV area/battery size combination of 12 modules / 16 kWh was observed from the economic, environmental, and technical viewpoints.

Keywords:

TRNSYS, Adsorption Cooling, Bioenergy, Food Cold Chain.

Graphical abstract

* corresponding author: aolabi@sharjah.ac.ae (A. G. Olabi)
* corresponding author: a.rezk@aston.ac.uk (Ahmed Rezk)

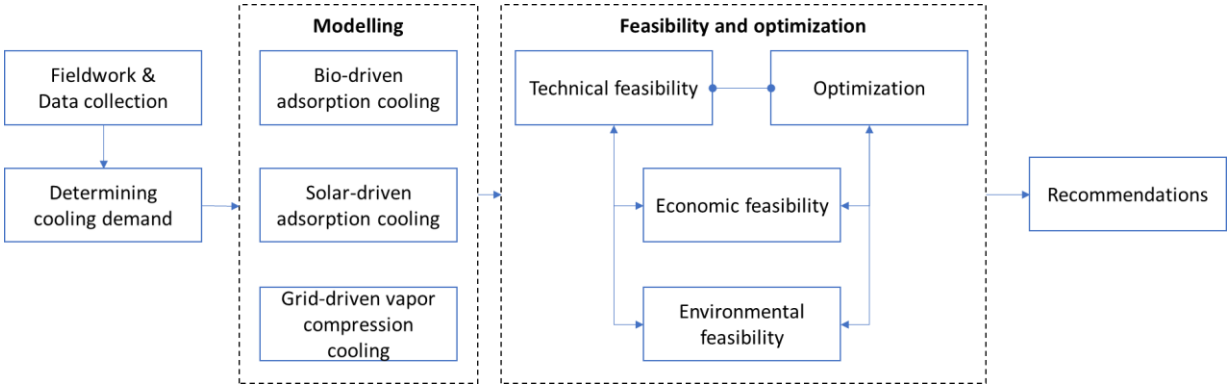

Highlights

- A standalone bio-driven adsorption cooling system was developed.
- A PV solar system was integrated to drive the system's auxiliaries.
- The system's variables were optimised to minimise the cost and environmental impact.
- The system's technical, economic, and environmental feasibility were analysed.

Nomenclatures

A	Collector area, m^2
B_{EC}	Battery energy storage capacity, Wh
C_{dp}	Crops exchange load, kg/day
C_{EC}	Cell energy capacity, Wh
COP	Chiller coefficient of performance
Cp	Specific heat capacity, kJ/kg K
CVCC	Conventional vapour compression chiller
ETC	Evacuated tube solar collector
FPC	Flat plat solar collector
SOC	State of charge
GHV	Gross heating value, MJ/h
H_c	Hydrogen content, %
IAM	Incident angle modifier, (°)
I_{sc}	Short-circuit current, A
I_{mp}	Current at maximum power, A
m	Biomass consumption rate, kg/h
$\dot{m}$	Mass flow rate, kg/h
MPTT	Maximum power point tracking
N_{CP}	Number of cells in parallel
	Number of cells in series

N_{CS}	Net heating value, MJ/kg
NHV	Electric chiller required power, kJ/h
P	Photovoltaic solar panel
PV	Energy rate, kJ/h
Q	Chiller capacity, kJ/h
Q_{cap}	Crops respiration cooling load, kJ/h
Q_{CL}	Crops respiration load, kJ/h
Q_{RL}	Collector useful energy, kJ/h
Q_u	Total incident solar energy, kJ/h/m^2
Q_t	
R_R	Respiration rate, W/kg
R_{SC}	Room storage capacity, kg
T	Temperature, $^{\circ}$C
T_{Isc}	Temperature coefficient of I_{SC}, A/K
TMY	Typical meteorological year whether file
TRNSYS	Transient system simulation
T_{Voc}	Temperature coefficient of V_{OC}, V/K
V_{mp}	Voltage at maximum power, V
V_{OC}	Open-circuit voltage, V
W_c	Water content, %
W_p	PV module power, W

Subscripts

b,in	Boiler inlet
c	Crops
chw	Chilled water
cw	Cooling water
d	Dry
hw	Hot water
i	Inlet
I_{SC}	Short-circuit current
mp	Maximum power
o	Outlet
p	Peak
OC	Open-ciruit
s	Set
SC	Short-circuit
VOC	Open-circuit voltage
w	Wet

Symbols

η_{col}	Solar Collector efficiency
η_{sys}	Total system efficiency
η_{boiler}	Boiler efficiency, %

1. Introduction

Food security is one of the most prominent global issues and is strongly linked to Food Waste and Losses (FWL). Globally, 33% of food production is wasted. FWL affects food security, profoundly affects the environment, and squanders the earth's precious resources. Globally, the uncontrolled food degradation in landfills emits 3.3 billion tons of environmentally harmful gases, such as methane and carbon dioxide. Aside from this, 250 km^3 of freshwater is wasted due to the irrigation of wasted crops. Out of 4.7 million hectares of agricultural land, about 1.4 million hectares are occupied by uneaten food [1-2].

In Sub-Saharan Africa (SSA), 37% of food is wasted at post-farming stages [3]. The lack of sustainable after-harvesting practices, such as cooling and drying, wastes 50% of fruits and vegetables at the farm level [4]. The lack of cooling in SSA is one of the leading causes of FWL. Therefore, developing sustainable cooling systems that utilise local resources to meet the farmers' demand for cooling is increasingly important [5]. Given that 65% of the population in SSA do not have access to grid electricity, specifically in rural smallholder farms, it is essential to utilise alternative and sustainable energy resources to securely drive the cooling chain, such as biological and solar energies [5]–[7].

Plant-based biomass is an alternative renewable energy resource that can provide thermal energy for various applications and be further processed to produce electricity. It is carbon-neutral, meaning the same amount of CO_2 absorbed by plants during their growing is emitted during their processing [8]. It also promotes circular economy principles, especially when converting agricultural wastes into energy, helping to manage natural resources sustainably [9], [10]. Amongst the wide range of tropical crops in SSA, bananas are the most popular. In Rwanda, the annual cultivated banana fruits are about 2 million tonnes and occupy about 165,000 hectares, representing about 23% of the total arable land [11]. Each ton of banana fruit produces 4 metric tons of banana residual, most of which are pseudostem but are still currently wasted. Therefore, utilising such biomass can potentially reduce its environmental impact and add value to the farming chain [12]–[15].

Building on the abundant banana agri-waste in many agricultural societies, there has been an increasing interest in exploiting it as a feedstock for various biorefineries- this would significantly reduce the waste

volume and the environmental damage caused by their disposal [12]–[15]. Banana agri-waste was converted to biomethane through biochemical conversion, otherwise dubbed anaerobic digestion. The influence of different parameters on biomethane production rate from banana agri-waste was widely investigated, including volatile solid loading rate, total solid concentration organic loading, pre-treatment type, and total solid content [16] [17] [18] [19]. It was reported that banana agri-waste digestion is technically feasible commercially and can provide a viable methane yield per volatile solid unit weight of bananas. However, the high moisture content of banana agri-waste significantly increased the digester's size. A recent study by Bhushan et al. [20] concluded that anaerobic digestion is more desirable than thermal and thermochemical conversion. The study highlighted the technical feasibility of utilising banana skin and rotten fruits as feedstocks to increase biomethane and ethanol fuel yielding.

With an emphasis on direct biomass combustion, the high moisture content of the agricultural residues, including banana agri-waste, delays combustion and limits its completion and stability. It is also logistically demanding to transport and store undried banana waste. As a result, hydrothermal treatment was introduced to remove the biomass moisture content at a lower temperature than the pyrolysis and gasification processes, using a water/steam medium. As a result, it increased the carbon content and heating value and reduced the ash content [21]. There are several CO2 capture methods, which exist at different levels of commercialisation, including physical and chemical absorption, adsorption, membrane, and cryogenics [22]. The emerging carbon capture technologies opened the door towards addressing the CO_2 emission released from biomass combustion. It led to other advanced combustion techniques, such as oxyfuel combustion, to intensify the CO_2 emissions and minimise other uncaptured emissions [23]. The oxyfuel combustion process mixes pure oxygen as an oxidant with recycled flue gases to control the excessive flame temperature, which leads to less harmful exhaust gases such as NO_x. This approach intensifies the CO_2 concentration up to 90-95% in the flue gas stream, where it is directly captured, stored, and utilised in other applications [24].

Solar is another abundant renewable energy source in SSA that can efficiently drive thermal-driven cooling systems (i.e., adsorption, absorption). Particularly, adsorption refrigeration systems are exemplified by utilising a wide range of low-grade driven temperatures and low environmental impact

[25], [26]. Solar thermal-driven cooling systems have been widely investigated both numerically and experimentally. Monne et al. [27] investigated the performance of a 4.5 KW-cooling Solar Thermal Driven Adsorption Cooling system (STDC-ads) integrated with 37.5 m^2 Flat Plate Solar Collectors (FPC) numerically, using the TRNSYS software. A strong relationship between the energy conversion efficiency of the system and the operating temperatures in the condenser and generator was reported. Sim [28] numerically optimised a 4.5 KW solar-assisted adsorption cooling system operated in Doha, Qatar using TRNSYS, where a reduction in the energy consumption of 47% compared to the conventional Vapour Compression Cooling system (VCC) was reported. The optimal solar collector area, collector tilt angle, and size of the heat storage tank were confirmed to be: 23.4 m^2, 24 deg, and 0.3 m^3.

Reda et al. [29] studied STDC-ads but operated in Assiut city, Egypt. It was observed that the solar fraction strongly depended on the collector area and heat storage size, but the solar fraction was hardly affected by the cold storage capacity. Generally, the adsorption cooling system can be driven by lower driving temperature, requires no liquid pump, and is more environmentally friendly than the absorption system. However, the performance of the absorption cooling system could outperform that of the adsorption system, specifically at high-grade heat.

There has been an emerging interest in utilising bioenergy in trigeneration systems to meet the increasing demand for power, heating, cooling, and other utilities in a carbon-neutral fashion, mainly in the most developed societies [30], [31]. Nevertheless, there has been little analysis of directly exploiting the thermal energy generated from locally sourced bioenergy, otherwise dubbed bio-heat, to address the lack of cooling that sits in the food-energy nexus and exacerbates due to the growing population in the developing societies. Therefore, this study compared the technical, economic, and environmental feasibility of driving adsorption cooling systems directly with the bioheat generated from directly combusting banana agri-waste and benchmarked it against solar thermal energy as a potential alternative to existing vapour compression refrigeration systems. These systems are driven by the grid electricity and built on the technical feasibility of utilising banana agri-waste as a feedstock in a range of biorefineries. The cooling demand was determined based on fieldwork undertaken in Rwanda's

selected geographical sites where off-grid cooling is needed. The integration between a cooling system, solar photovoltaic system, direct biomass combustion using oxyfuel approach and the metrological data and its influence on the transient cooling demand was simulated using TRNSYS commercial software, owing to its validity and versatility to study various integrated systems [32]. To the best of the authors' knowledge, no single study exists that investigated the technical, economic, and environmental feasibility of such a range of integrated systems to understand the feasibility of exploiting local biomass to meet the cooling demand of those most in need.

2. Systems modelling

Three systems were simulated and benchmarked: a solar-driven adsorption cooling system, a bio-driven adsorption cooling system, and a vapour compression cooling system driven by grid electricity. It is noteworthy that a PV-driven vapour compression system was not included, albeit its strong techno-economic potential, due to concerns about using conventional refrigerants of high adverse environmental impacts. The primary components of the adsorption cooling system were the adsorption refrigeration unit, heat storage, cold storage, cooling coil, dry cooler, and cold room. Circulating pumps were used to circulate heating, cooling, and chilled water. Solar thermal energy was the heat source in the solar-driven cooling system and was harvested by evacuated tube solar collectors. The direct combustion of agricultural waste, primarily banana agri-waste in the bio-boiler, was the heat source in the bio-driven cooling system. Both adsorption cooling systems were integrated with a solar PV system to power the electric components such as pumps and control. The primary components of the vapour compression cooling system were the electrically driven refrigeration unit, cooling coil, and cold room. The nominal performance of the vapour compression system is shown in figure 1. Each system was designed to meet the cooling demand required to preserve a range of perishable products at a farm level in an existing cold room of 13 m^2 floor area × 2.9 m height, located in Kigali, Rwanda. A commercial simulation tool (TRNSYS 18) was employed to simulate the year-round transient operation of each cooling system. The schematic diagrams of the simulated systems, including TRNSYS components, are presented in Figures (2-4).

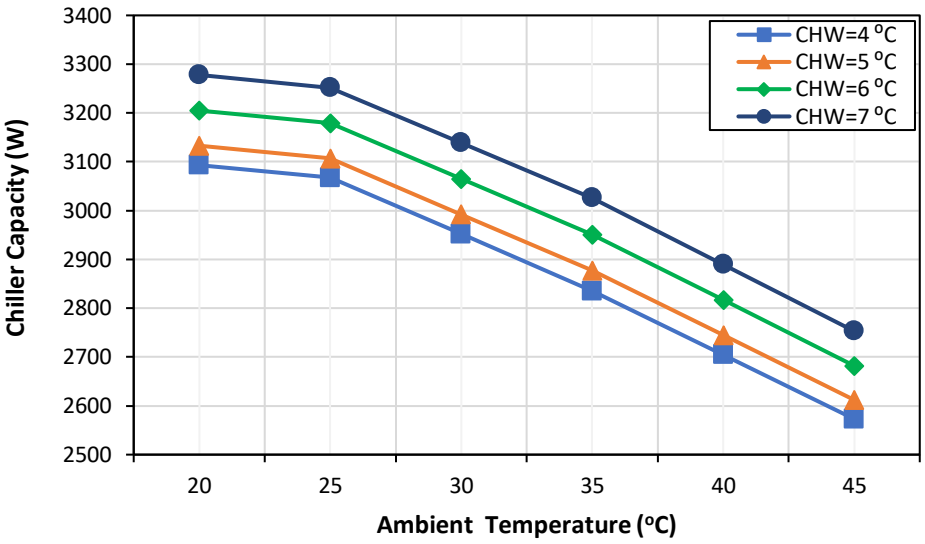

Figure 1. The nominal performance of the vapour compression refrigeration unit.

2.1. Weather data

The hourly-based meteorological data throughout the year for a broad range of geographical sites worldwide is available in TRNSYS through a database file (TMY2). In the present study, the hourly typical meteorological data for Kigali, Rwanda was processed by TRNSYS weather component (Type 15) and connected to other relevant components such as solar collector, hot and cold storage, biomass boiler, PV array, dry cooler, and the cold room as shown in Figures 2 and 3 [33].

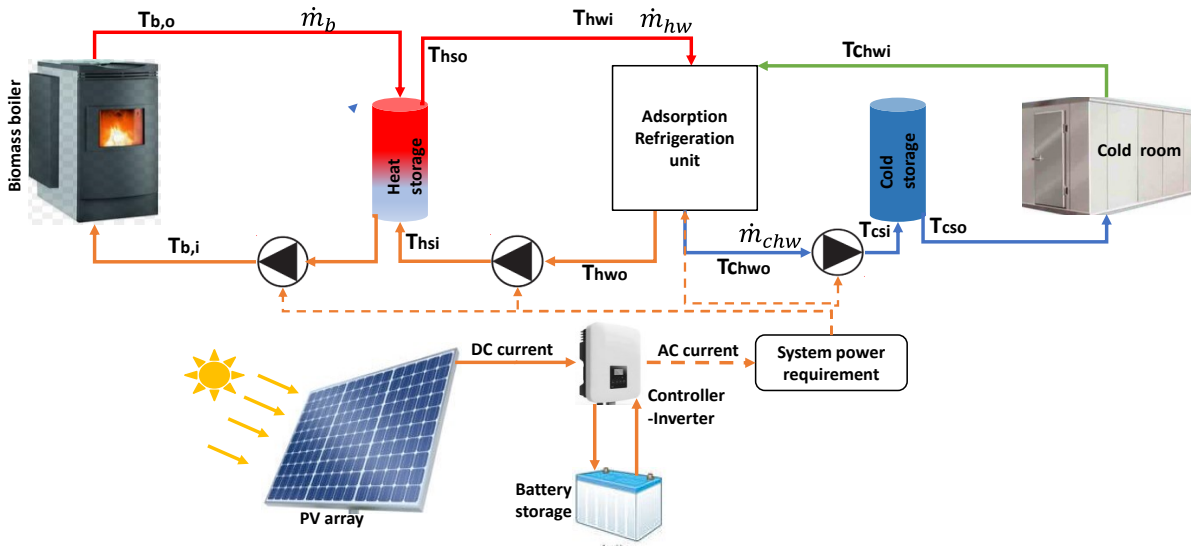

Figure 2. Schematic diagram of biomass heat-driven refrigeration system connections

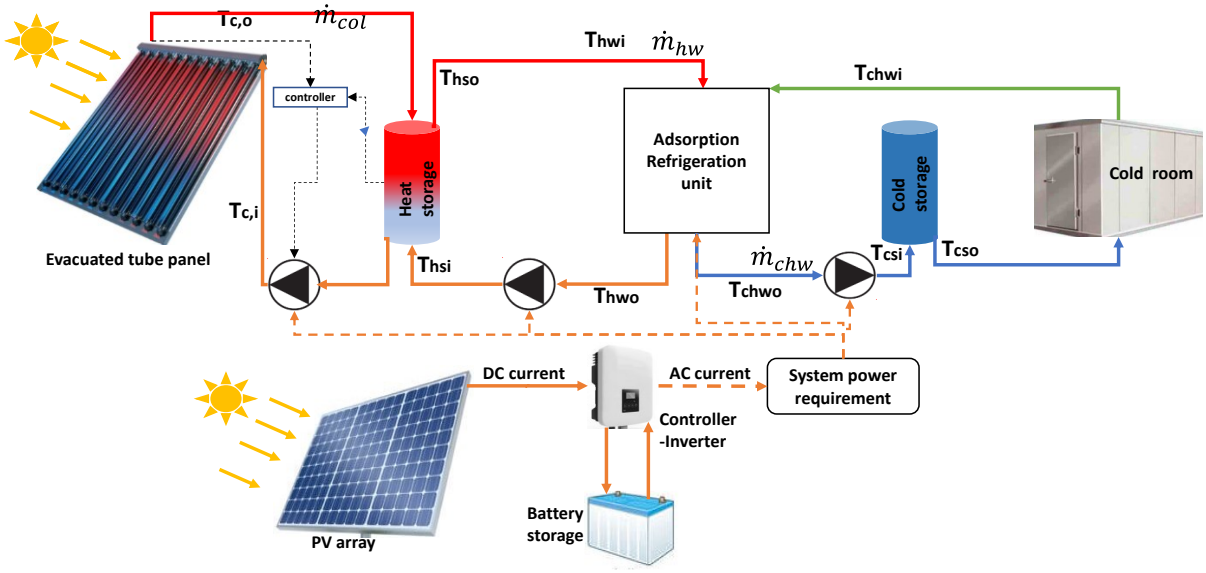

Figure 3. Schematic diagram of solar thermal-driven refrigeration system

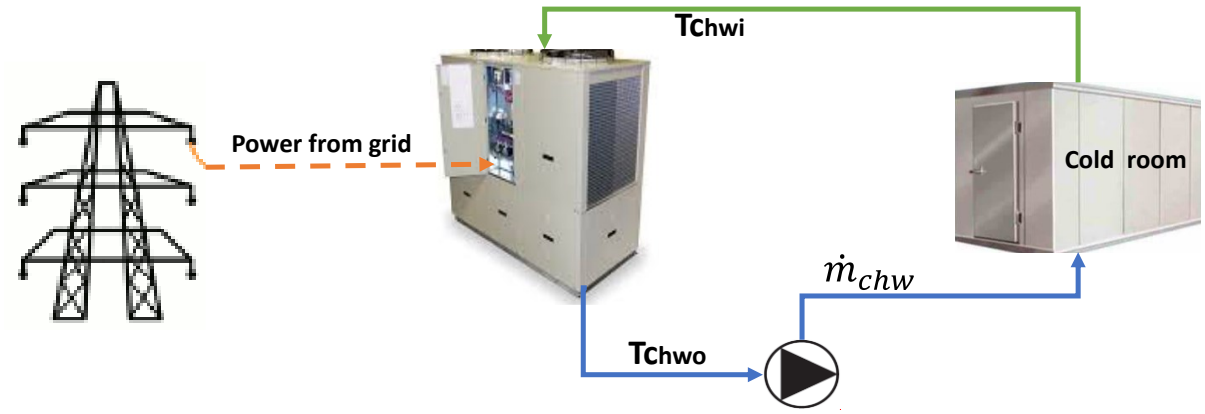

Figure 4. Schematic diagram of grid electricity-driven vapour compression refrigeration system

2.1. Cooling demand

2.1.1 Cooling load

There are three sources of the transient cooling load: heat gain, crop daily loading, and crop respiration rate. Figure 5 presents the programming flowchart for determining the transient thermal behaviour of the cold room. TRNSYS3D sketching tool (Trnsys3d) was coupled with google SketchUp to define the built room description that was then imported to TRNBuild to be processed and exported to TRNSYS building component (Type 56) in the TRNSYS simulation environment [34]. Various building features, such as building materials, orientation, external and internal heat gains, ventilation, infiltration rate, and building set humidity and temperature, can be interpreted using Multizone building modelling, with TRNBuild coupled with building component (Type 56). The developed building component (Type 56)

generates the outputs required by the modelled cooling system (e.g., temperature, humidity, sensible cooling load) to maintain the room setting conditions.

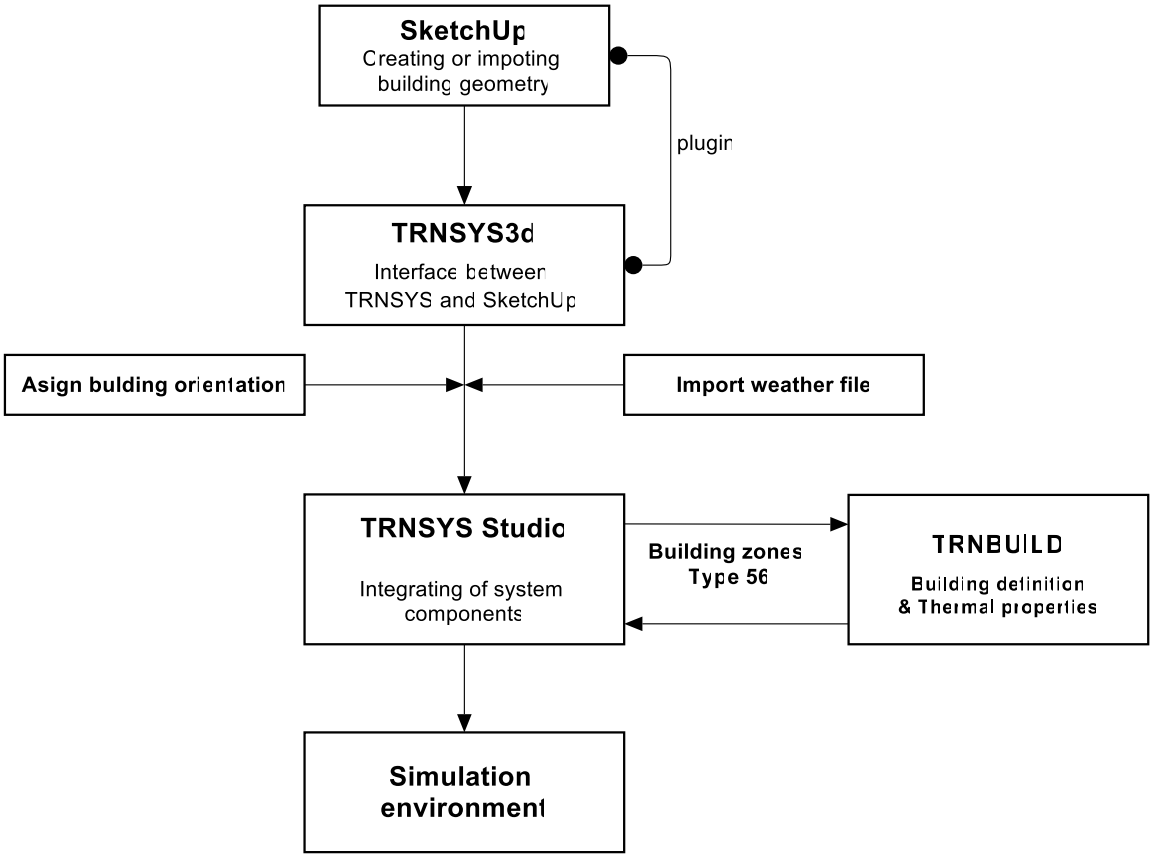

Figure 5. Interfaces used in TRNSYS to build zone model.

2.1.2 Cold storage operating conditions

Table 1 presents the fieldwork outcomes undertaken in Kigali and Nyagatare in Rwanda to gather data about temperature-sensitive crops. Nyagatare is located in the eastern province and represents the farming location, as farming is the primary occupation of the population. On the other hand, Kigali represents the central trading market in Rwanda. Therefore, having a cold chain connecting the farming location and the central markets is necessary. The fieldwork included 90 agribusiness workers, such as farmers, market traders, distributors, and suppliers. Based on the preferable storage conditions, the average temperature and humidity of the cold room were chosen to be 10 °C and 90% RH [35]. These operating conditions ensure the usability of the cold storing approach at the community level throughout the year.

Table 1. The crops verity in Rwanda and the recommended storage conditions [35]

Crops	Storage temperature °C	Storage humidity %	Postharvest life/approx.
Storage temperature range around 10 °C			
Tomatoes			
Mature, green	10-13	90-95	2-5 weeks
Firm, ripe	8-10	85-90	1-3 weeks
Pepper	7-10	95-98	2-3 weeks
Mango	13	85-90	2-3 weeks
Melon- Casaba	7-10	85-90	3-4 weeks
Orange	5-10	85-90	12 weeks
Papaya	7-13	85-90	1-3 weeks
Passionfruit	10	85-90	3-4 weeks
Bananas	10-13	90-95	1-4 weeks
Cucumber	10-12	85-90	10-14 days
Avocadoes	13	85-90	2 weeks
potatoes	10-15	90-95	10-14 days
Eggplant	10-12	90-95	1-2 weeks
Pineapple	7-13	85-90	2-4 weeks
Storage temperature sub 10 °C			
Apple	-1-4	90-95	1-2 months
Carrots	0	98-100	3-6 months
Onions	0	65-70	
Cabbage	0	95-100	2-3 months
Beans	0	90-95	1-2 weeks
Strawberry	0	90-95	7-10 days

The crops' cooling load was simulated as an additional heat gain in the TRNSYS building component (Type 56), which considered crops daily loading, including field heat and crops respiration. The loading density was considered 3.75 m^3 per metric ton to determine the heat gained from crops' daily loading [36]. Given the cold store volume of 38 m^3 (13 m^2 floor area × 2.9 m height), the room storage capacity was determined as 10 tons. Accordingly, the heat gain because of the crops loading can be determined using Equation 1:

$$Q_{CL} = \frac{C_{dR} \times Cp_c \times \Delta T}{24} \qquad kJ/h \qquad (1)$$

Q_{CL} denotes crops exchange cooling load, C_{dR} is the crops' daily rate, Cp_C is the crops' specific capacity, and ΔT is the temperature difference between the crops loading temperature and the room set temperature. The respiration cooling load is calculated using Equation 2 and values from Table 2:

$$Q_{RL} = R_R \times (R_{SC} - C_{dR}) \times 3.6 \qquad kJ/h \qquad (2)$$

Q_{RL} is the crops' respiration load, R_R is the crops respiration rate, and R_{SC} is the room storage capacity. The constant values in equations 1-2 are furnished in table 2 and according to Paranjpey [36] and Faith et al. [37].

Table 2. Crops data and cooling load

Items	Value	Units	Ref.
Daily crops loading percentage	4-5	%	[36]
Daily loading rate	400-500	kg/day	-
Crops specific heat	3.7	kJ/kg. K	[37]
Crops initial temperature	20	˚C	-
crops respiration rate	0.0179	W/kg	[37]
crops exchange cooling load	771	kJ/h	Eq.(1)
Crops respiration load	612	kJ/h	Eq.(2)

Therefore, crops' cooling load of 1383 kJ/h was added to the zone model to determine the gross cooling demand of the cold room. Figure 6 presents the ambient temperature and the cooling demand per unit area of the cold room throughout the year resulting from the cooling load calculations.

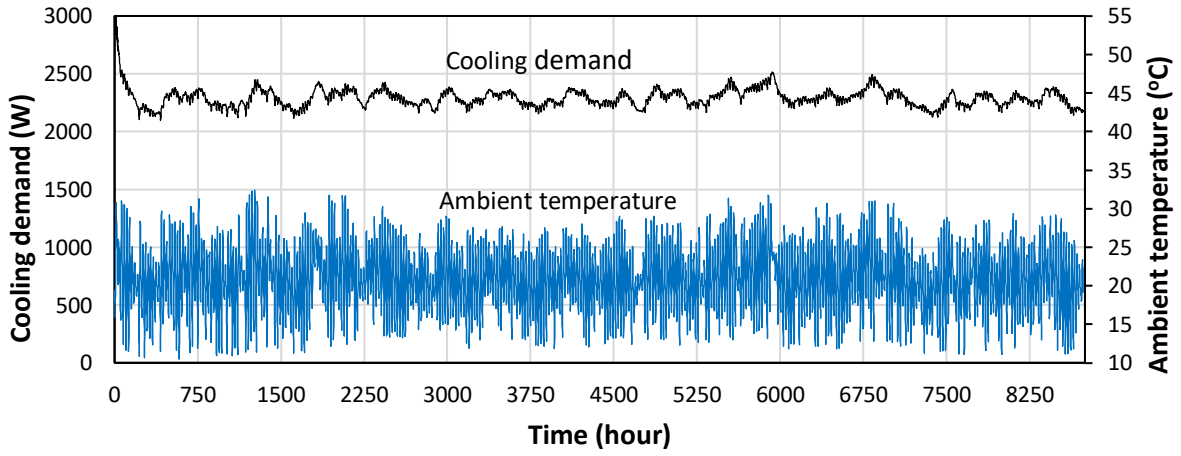

Figure 6. Hourly variation of cooling demand and ambient temperatures throughout the year

2.3. Heat sources

2.3.1. Bio-boiler

The bio-boiler that utilised banana residual as biomass was simulated using the TRNSYS boiler component (Type 122) and is shown in Figure 7. The bioheat released from combusting dry and wet banana biomass can be determined using Equation 3-4 according to Haller et al. [38].

$$NHV_d = (GHV_d - 2.442(9.079 \times H_c + W_c)) \times 1000 \qquad kJ/kg \qquad (3)$$

$$NHV_w = \frac{GHV_d - 2.442(9.079 \times H_c + W_c)}{1 + W_c} \times 1000 \qquad kJ/kg \qquad (4)$$

Where NHV_d and NHV_w denote net heating values for dry and wet biomass fuel, respectively, GHV_d is the gross heating value of dry fuel, H_c biomass hydrogen content, and W_c biomass water contents. GHV, Hc, and Wc values for banana biomass are based on a 75/25 pseudostem/leaves & peels ratio to represent the actual banana waste components and are furnished in table 3- building on previous work done by Kabenge et al. [13]. 20% of the boiler output energy was used to imitate the energy demanded by the CO_2 capture unit [39] [40] [41]. The air separation unit, supplying pure oxygen for the combustion process, consumes about 60% of the energy required for the carbon capture process because cryogenic distillation demands a high amount of energy [42]. The consumption rate of biomass is directly proportional to the boiler inlet energy and inversely proportional to NHV_d and NHV_w, which can be determined using Equations 5-6:

$$m_d = \frac{Q_{b,in}}{NHV_d} \qquad kg/h \qquad (5)$$

$$m_w = \frac{Q_{b,in}}{NHV_w} \qquad kg/h \qquad (6)$$

Where m_d and m_w are the dry and wet biomass fuel consumption rates, respectively, and $Q_{b,in}$ is the boiler inlet energy. Equations 3-6 were imported to the TRNSYS boiler component to determine the fuel consumption, according to the thermal energy required to drive the refrigeration system to meet the cooling demand.

Table 3. Characteristics of dry banana biomass waste [13]

Item	Peels	Leaves	Pseudostem
W_c %	11.56	6.67	7.98
H_c %	6.19	6.44	6.44
GHV_d MJ/kg	16.15	17.57	15.04

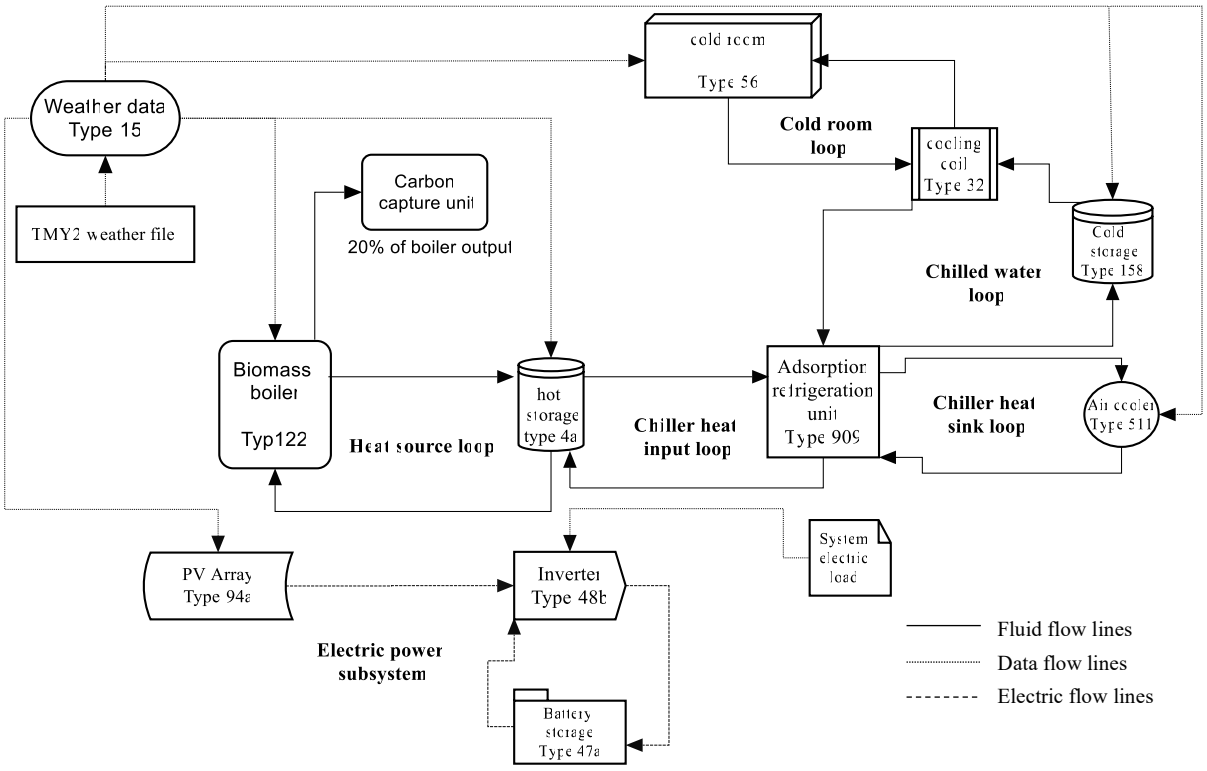

Figure 7. Flow chart of main integrated subsystems and their connections to biomass driven cooling system.

2.3.2. Solar thermal energy

Evacuated Tube Solar Collector (ETC) arrays were employed to harness the solar thermal energy required to drive an adsorption refrigeration system. It was simulated using the TRNSYS solar thermal collector component (Type 71), shown in Figure 8. A solar thermal collector component employs a standard quadratic efficiency equation that considers the asymmetry of the ETC in the design of the optical model. It interpolates the Incident Angle Modifier (IAM) value from an external data file, based on the traverse and longitudinal angles of the incident radiation on ETC. The optical efficiency (80%), first loss coefficient (1.5 $W/m^2.K$), and second loss coefficients (0.0016 $W/m^2.K$) were identified based on the work done by Khan et al. [43]. This study optimised the collector area, collector slope, and hot water flow rate to maximise hot water temperature, collector efficiency, refrigeration system performance, and maintain the cold room at the desired conditions. Other inputs, such as metrological

data and collector inlet water temperature, were directly determined through coupling the TRNSYS solar thermal collector component to weather and heat storage components. The collector efficiency (η_{col}) was determined by dividing collector valuable energy (Q_u) by total collector area A, Equation (7):

$$\eta_{col} = \frac{Q_u}{Q_t\, A} \tag{7}$$

2.4. Refrigeration system

2.4.1 Adsorption refrigeration system

The adsorption refrigeration system was simulated using the TRNSYS adsorption chiller component (Type 909), which employed a normalised lookup table to determine the performance of the adsorption refrigeration system at given operating conditions. The energy of the chilled water (Q_{chw}) was determined based on the minimum of refrigeration unit capacity and the chilled water energy, as shown in equation (8), [44]:

$$Q_{chw} = \min\left(Q_{cap}, \left(\dot{m}_{chw}\, Cp_{chw}\left(T_{chw,i} - T_{chw,s}\right)\right)\right) \qquad kJ/h \tag{8}$$

Q_{cap} is the refrigeration unit capacity, which is set as input (3 kW) according to the cooling demand. $\dot{m}_{chw}$, Cp_{chw}, $T_{chw,i}$, and $T_{chw,s}$ are the mass flow rate, specific heat, inlet temperature, and setpoint outlet temperature of the chilled water. The chilled water flow rate $\dot{m}_{chw}$ was controlled to maintain the room temperature at 10 ºC and in response to the dynamic cooling demand. The refrigeration fan coil unit was simulated using the TRNSYS cooling coil component (Type 32) coupled with a fan component (Type 146). $T_{chw,s}$ was set as an input to the module. If the chiller input conditions at the current time step could be achieved, $T_{chw,s}$ was fixed to the set value; if not, $T_{chw,s}$ set value was increased to a particular value depending on the inlet conditions.

The heat energy (Q_{hw}) required to operate the adsorption refrigeration unit, the heat removed to the ambient (Q_{cw}), hot water outlet temperatures of the hot water ($T_{hw,o}$), and cooling water ($T_{cw,o}$) were determined using energy conversation law, Equations 9-12:

$$Q_{hw} = \frac{Q_{chw}}{COP} \qquad kJ/h \tag{9}$$

$$Q_{cw} = Q_{hw} + Q_{chw} \qquad kJ/h \tag{10}$$

$$T_{hw,o} = T_{hw,i} - \frac{Q_{hw}}{\dot{m}_{hw}\, CP_{hw}} \quad °C \quad (11)$$

$$T_{cw,o} = T_{cw,i} + \frac{Q_{cw}}{\dot{m}_{cw}\, CP_{cw}} \quad °C \quad (12)$$

Where $T_{hw,i}$ is the chiller inlet hot water temperature from the heat storage. $T_{cw,i}$ is the condenser cooling temperature admitted from an air cooler simulated by TRNSYS dry cooler component (Type 511), more details about obtaining the COP and other parameters are found in [44]. The actual ambient condition was considered by coupling the dry cooler component with the weather data. Figure 7 presents all components of the solar thermal-driven refrigeration system. Equation 13 presents the overall system efficiency of solar-driven adsorption cooling system (η_{sys}) based on ETC efficiency (η_{col}) and the refrigeration coefficient of performance.

$$\eta_{sys} = (\eta_{col}\, or\, \eta_{boiler}) \times COP \quad (13)$$

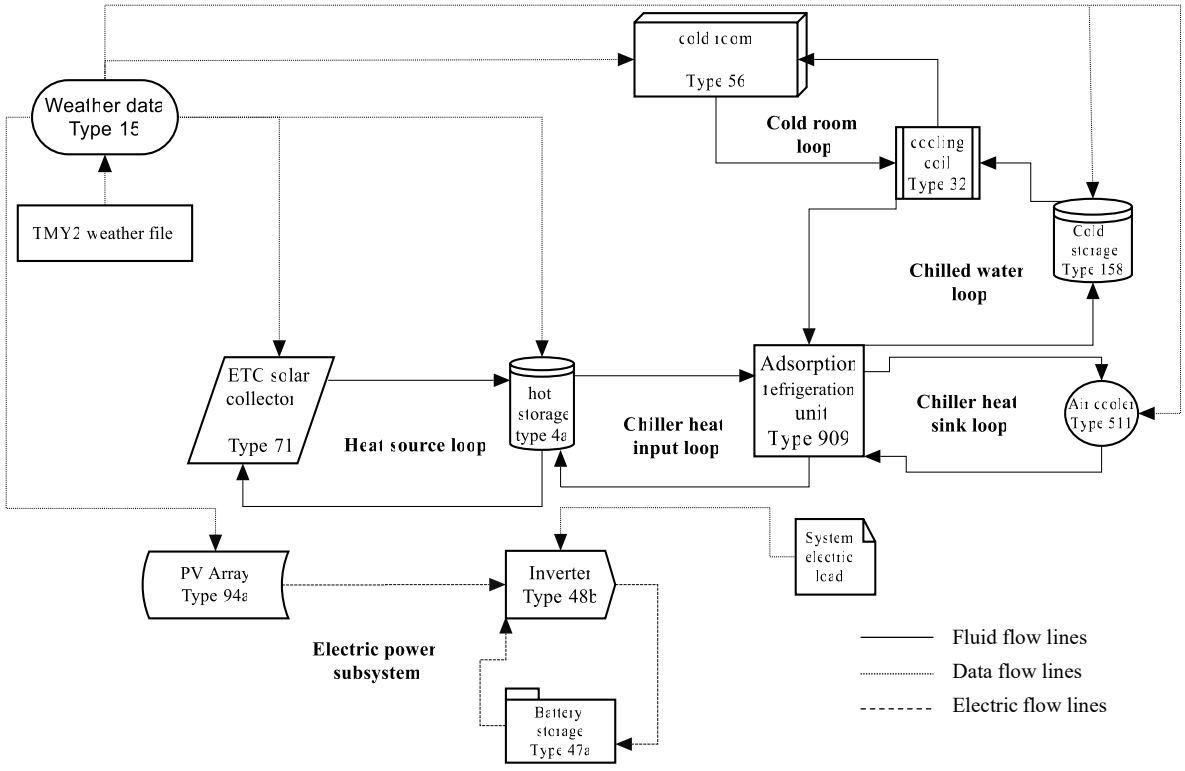

Figure 8. Flow chart of main integrated subsystems and their connections for solar-driven cooling system

2.4.2 Vapour compression refrigeration system

A digital twin was developed to an existing vapour compression refrigeration unit, driven by the grid electricity. The TRNSYS module air-cooled chiller (Type655) simulated the vapour compression refrigeration machine by predicting its performance depending on an impeded lookup table. Other

system components, such as the fan coil and the cold room, were similar to those used in the adsorption refrigeration system, as shown in Figure 9. The chilled water energy Q_{chw} (chiller load) was determined using equation (14):

$$Q_{chw} = \dot{m}_{chw}\, Cp_{chw} \left(T_{chw,i} - T_{chw,s}\right) \qquad kJ/h \qquad (14)$$

Accordingly, the electric power drawn by the chiller's compressor (P) from the electricity grid was calculated as in equation (15); more details about obtaining the COP and other parameters are found in [44]:

$$P = \frac{Q_{chw}}{COP} \qquad kJ/h \qquad (15)$$

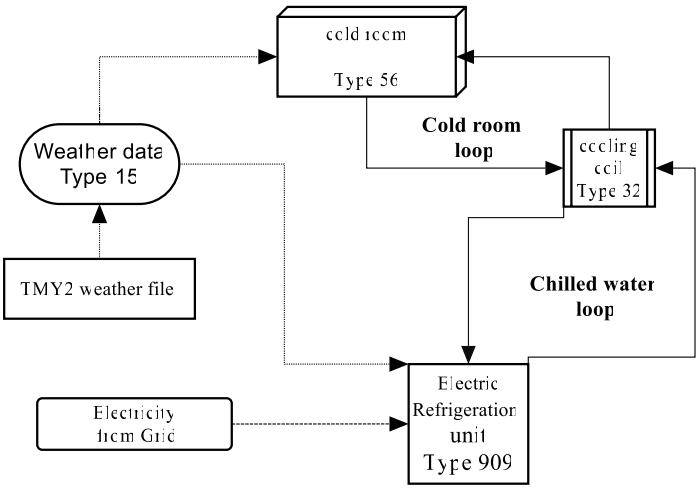

Figure 9. Flow chart of main integrated subsystems and their connections for grid electricity-driven cooling system

2.5 Thermal-energy storing

Heat or cold storage mediums are stored by applying thermal energy technologies using different conditions, namely, temperature, place and power [45]. Heat and cold storage are required to steady the solar thermal and bio-boiler-driven refrigeration systems and store sufficient thermal energy to run the solar thermal-driven refrigeration system 24/7 throughout the year. As such, hot- and cold-water storage were simulated using the TRNSYS stratified storage tank components (Type 4a) and (Type158), as presented in Figures 7-8. The hot storage volume was optimised depending on the solar collector area to balance system performance and provide adequate heat for continuous operation. Subsequently, the

cold storage volume was mounted to provide the highest system performance and maintain the cold room temperature at 10 °C.

2.6. Photovoltaic solar energy

Although adsorption refrigeration systems are thermally driven, pumps and control units require electric energy. Therefore, a PV/battery subsystem was integrated into the adsorption refrigeration system to meet the demand for electric energy and maintain its operation 24/7 throughout the year, as shown in Figures 2 and 3. The electrical performance of the PV panel was simulated using the TRNSYS Photovoltaic component (Type 94a). The electrophysical parameters defining the simulated PV array are furnished in Table 4, according to commercially available polycrystalline solar panels produced by PEIMAR [46].

The TRNSYS regulator/inverter component (Type 48b) and battery component (Type 47) were used to regulate and store the electric energy generated by the Photovoltaic component, as shown in Figures 7 and 8. The regulator element controlled the PV power and the battery charging / discharging processes at an efficiency of 78%, while the inverter element converted the power dispatched to the load from DC into AC power at an efficiency of 96% [47]. The Maximum Power Point Tracking (MPPT) technique was used to maximise the power extraction of the PV array, which monitored the battery State-of-Charge (SOC) and tracked the PV power, rather than the voltage. The high and low limits on Fractional State-of-Charge (FSOC), a parameter that defines the ratio of the stored energy divided by the overall storage capacity of the battery, were set to 1 and 0.3, respectively; this prioritised the battery charging and prevented discharging at SOC lower than 0.3 [48]. The battery efficiency was set as 90%, according to Wang and Deniss [47]. Equation 16 presents the electric energy storage capacity (B_{EC}) as a function of each cell capacity (C_{EC}- Wh), the number of cells in parallel (N_{CP}), and the number of cells in series (N_{CS}) [49].

$$B_{EC} = C_{EC} \times N_{CP} \times N_{CS} \qquad Wh \qquad (16)$$

Table 4. PV panel parameters.

Parameter	W_p	**Area**	V_{mp}	V_{OC}	I_{mp}	I_{sc}	T_{Isc}	T_{Voc}	**# Cells**
Units	W	m^2	V	V	A	A	A/K	V/K	
Value	280	1.6	31.2	37.3	8.98	9.7	0.04	-0.079	60

2.7 Optimisation of biomass system

The GenOpt software was employed to optimise the biomass system parameters, using TRNOPT as an interface between GenOpt and TRNSYS, as demonstrated in Figure 10. The Hooke–Jeeves algorithm was used to solve the optimisation problem in a dynamic fitness landscape at relatively low computational intensity instead of other available algorithms, such as particle swarm optimisation and hybrid global optimisation.

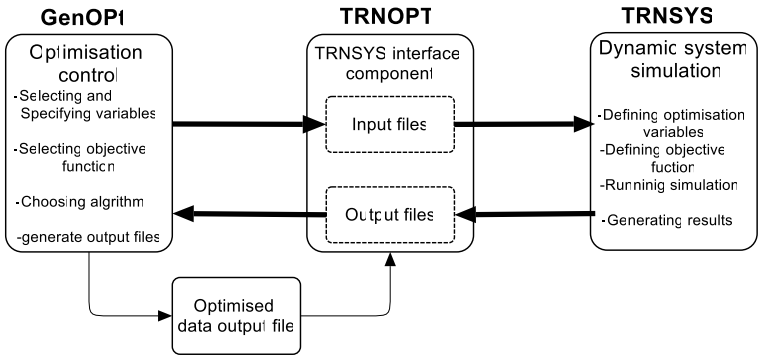

Figure 10. Flow chart of the optimisation process

The objective function is biomass fuel consumption. It is highly dependent on bio-boiler inlet energy and biomass heating value, as represented by equation-5. Table 5 shows the optimisation variables, constraints, and initial values to operate the algorithm. The optimisation algorithm optimises these variables, aiming at the lowest biomass consumption and constrained by delivering a maximum system performance while maintaining the cold store at the desired conditions. After determining the minimum fuel consumption, GenOpt was used to perform a parametric optimisation to examine the effect of system variables on the biomass fuel consumption rate and the system performance.

Table 5. Optimisation variables of biomass system

Variables	Minimum value	Maximum value	Initial value
Boiler set temperature (°C)	65	100	90
Boiler hot water flow rate (kg/h)	50	1000	500
Heat storage volume (m^3)	0.001	1	0.1

3. Results and discussion

3.1 Modelling verification

TRNSYS is a mathematical solver widely employed for simulating transient energy systems. Other researchers previously used components used in the present study, and most of them validated within 10% average deviation, as presented in table 6.

Table 6. System's components used in this work and validated in the literature

TRNSYS component	Reference
Solar thermal collector (Type 71)	[29], [50], [51]–[53]
Heat storage tank (Type 4)	[27], [29], [50], [51]–[53]
Cold storage tank	[29], [51], [52]
Cooling coil	[27], [29], [50], [51]
Weather component	[29], [50], [49], [52]
Multizone building (Type 56)	[29], [51]
Electric chiller (Types 655 and 666)	[54]
PV panel (Type 94)	[47], [48], [54], [55]
Controller-Inverter (Type 48)	[47], [48], [54], [55]
Battery storage (type 47)	[47], [48], [54], [55]

In figure 11, the "Inlet-heat" denotes adsorption chiller heat input, "Pred" and "Actual" are the result predicted by the current study and the experimental data from the literature, respectively. The predicted performance was compared with the experimental data of a commercial adsorption chiller previously investigated by Rezk [56] to validate the TRNSYS adsorption chiller component (Type 909). As shown in Figure 11, a good agreement between the predicted and experimental data can be observed, where the maximum deviation was below 3% for COP, 6.8% for chiller capacity, and 7.2% for chiller inlet heat.

The silica gel/water adsorption cooling system was employed in this study, which provided the cooling required to preserve a wide range of crops at 7-13 °C. Freezing cannot be achieved using water as a refrigerant, Fang et al. [57]. Although other crops such as carrots and onions require lower preservation temperatures (0-5 °C), a silica gel adsorption chiller can still be employed to absorb the field

temperature before preserving such crops (pre-cooling). This contributes significantly to prolonging the shelf life. Investigating the pre-cooling required or low-temperature preservation for such crops was not in the scope of this study.

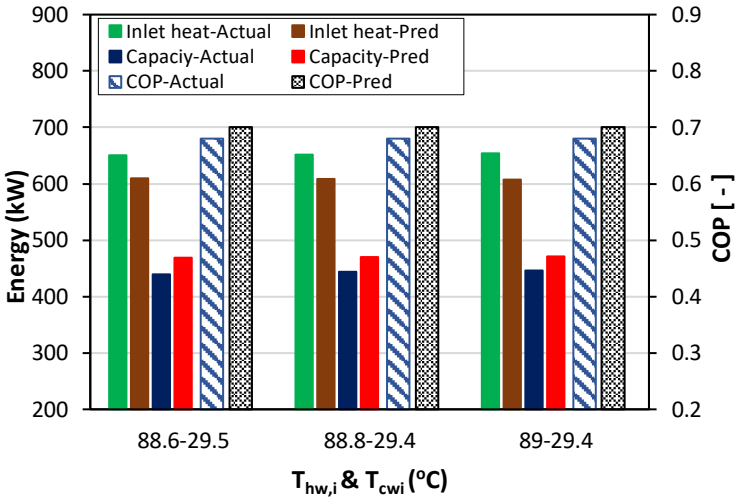

Figure 11. Chiller model validation (a) COP (b) chiller capacity and (c) chiller heat input

3.2. Bioenergy-driven cooling system

The adsorption cooling system was integrated with a bio-boiler, powered by banana agri-residual combustion, including banana peels, leaves, and pseudostems. Each ton of banana fruit produced about 4 tons of banana agri-residual, about 75% pseudostems, 13% peels, and 12% leaves [12]. The moisture content of dry banana residuals was about 8.3%, as shown in Table 3 [13]. In this study, the operating parameters, such as boiler setting temperature, boiler hot water flow rate, and hot water storage size, were optimised, aiming at the lowest possible biomass consumption and highest chiller performance while maintaining the cold store at 10 °C. As mentioned earlier, the air cooler was used to release the heat to the ambient; hence, the heat sink temperature varies with the ambient temperature fed by the year-round atmospheric conditions.

Generally, the boiler heat transfer rate depends on the flow rate and the temperature difference. For the give case study, the cooling demand from the heat-driven refrigeration system varies, affecting the boiler performance and the overall COP. Therefore, it was necessary study the effect of increasing the boiler supply temperature (B-SET-TEMP) and its impact on the COP. As such, Figure 12 presents the influence of varying hot water flow rates on biomass consumption, COP, chiller inlet temperature,

chiller heat input, and chiller maximum possible capacity at different boiler set temperatures (B-SET-TEMP) and a heat storage volume of 0.01 m^3. The COP presented in figure 12b is based on the actual cooling demand at the given operating condition. In the current study, low temperatures like 60 and 70 ^oC were used because the adsorption refrigeration unit is characterised by running at relatively low temperatures such as 60 ^oC. It can be observed that increasing the hot water mass flow rate decreases the daily biomass consumption to a certain point and then remains constant for all boiler set temperatures. This case study's minimum dry biomass consumption was 36 kg/day, corresponding to a hot water flow rate of 601 kg/h and a boiler set temperature of 95.

Meanwhile, the maximum was 51 kg/day at 350 kg/h and 70 $^{\circ}C$. This can be attributed to the contradicting trend of the COP by varying the hot water mass flow rate (figure 12b), where increasing the hot water flow rate in the boiler loop increases the chiller inlet hot water temperature at a fixed hot water flow rate in the chiller loop, as shown in figure 12c. Increasing the COP decreased the chiller heat input, as presented in Figure 12d. The boiler required inlet heat also decreased, which reduced the biomass consumption rate. A similar reason was behind the reduction in biomass consumption when the boiler set temperature increased.

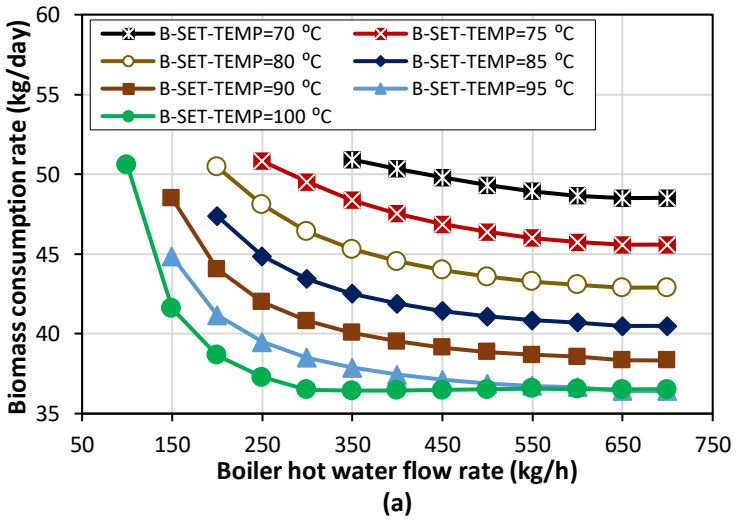

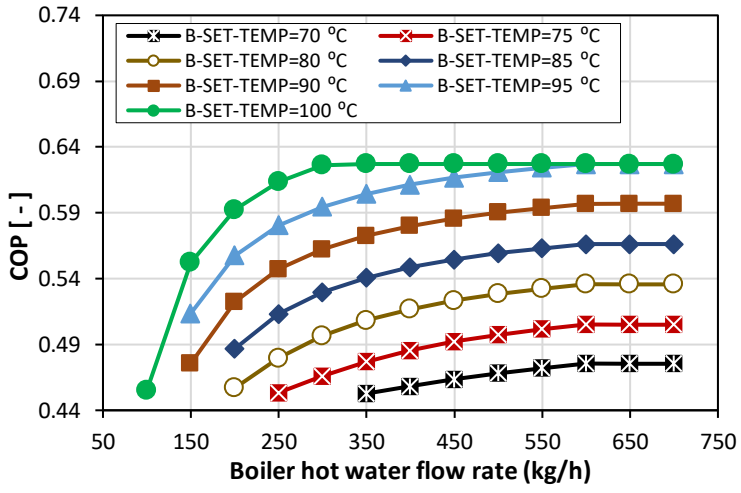
B-SET-TEMP=70 °C
B-SET-TEMP=75 °C
B-SET-TEMP=80 °C
B-SET-TEMP=85 °C
B-SET-TEMP=90 °C
B-SET-TEMP=95 °C
B-SET-TEMP=100 °C
COP [-]
0.74
0.69
0.64
0.59
0.54
0.49
0.44
50
150
250
350
450
550
650
750
Boiler hot water flow rate (kg/h)

(b)

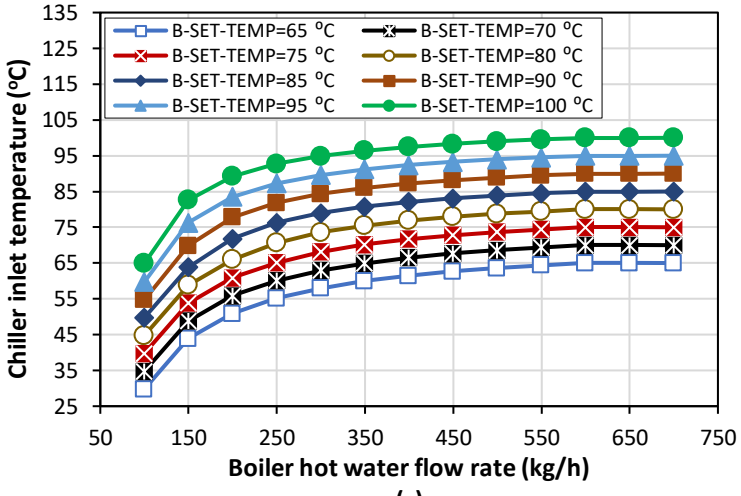
B-SET-TEMP=65 °C
B-SET-TEMP=70 °C
B-SET-TEMP=75 °C
B-SET-TEMP=80 °C
B-SET-TEMP=85 °C
B-SET-TEMP=90 °C
B-SET-TEMP=95 °C
B-SET-TEMP=100 °C
Chiller inlet temperature (°C)
135
125
115
105
95
85
75
65
55
45
35
25
50
150
250
350
450
550
650
750
Boiler hot water flow rate (kg/h)

(c)

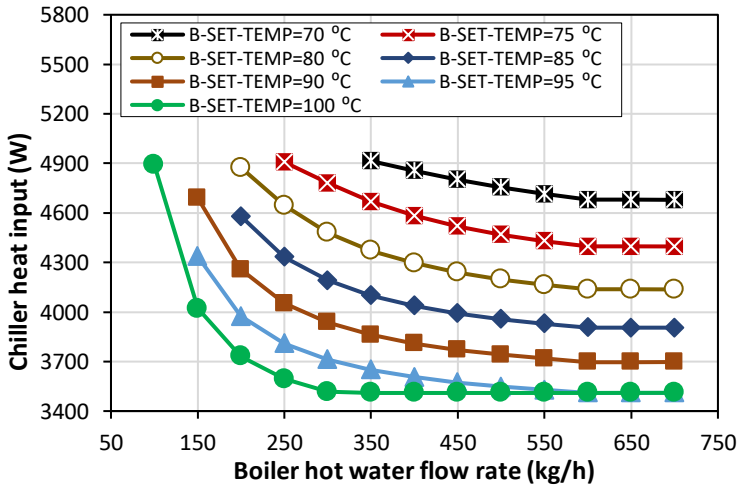
B-SET-TEMP=70 °C
B-SET-TEMP=75 °C
B-SET-TEMP=80 °C
B-SET-TEMP=85 °C
B-SET-TEMP=90 °C
B-SET-TEMP=95 °C
B-SET-TEMP=100 °C
Chiller heat input (W)
5800
5500
5200
4900
4600
4300
4000
3700
3400
50
150
250
350
450
550
650
750
Boiler hot water flow rate (kg/h)

(d)

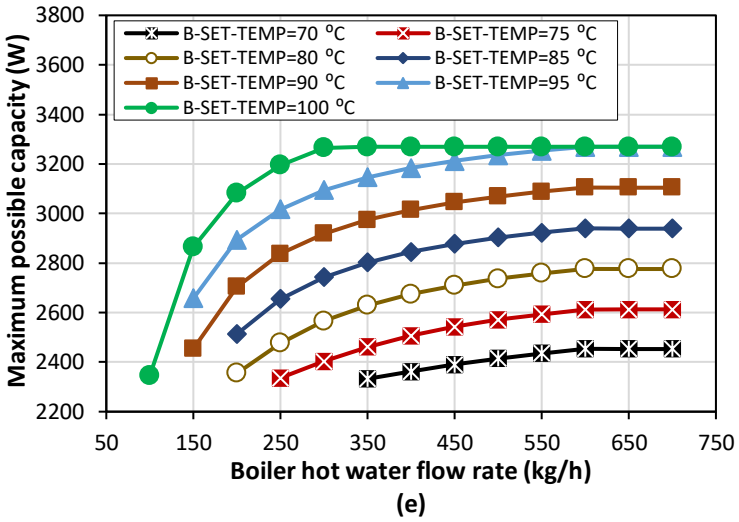

Figure 12. Effect of hot water flow rate on (a)-biomass consumption rate, (b)-COP, (c)-chiller inlet temperature (d)-chiller input energy, and (e)-chiller maximum possible capacity at different boiler set temperatures and 0.01 m^3 heat storage volume

Further increases in the boiler hot water flow rate after the optimum value of 601.25 kg/h did not affect the biomass consumption or the system performance due to the almost constant chiller loop heating temperature for all boiler set temperatures. It was also noticed that after the boiler hot water flow rate of 600 kg/h, increasing the boiler set temperature from 90 to 100 ˚C did not further decrease the biomass consumption within the investigated range because COP plateaued. Consequently, boiler heat input and the chiller capacity remained almost the same for both temperatures. Although the COP decreased at low heating temperature due to the insufficient refrigerant circulation and low cooling capacity, excessively hot water inlet temperature would typically lead to a build-up of heat stored in the adsorption beds. This negatively affects energy conversion efficiency during the adsorption/desorption [56], [58]. Absorbing the excess heat into thermal energy storage at the interface between the chiller loop and boiler loop enables plateauing of the COP for wider ranges of heat source temperatures.

The non-woody biomass straw average consumption reported by Sher et al. [23] was 0.2 kg/h per kW of boiler capacity (i.e., 4 kg/h per 20 kW). Taking 18.21 MJ/kg heating value of straw 13.87 MJ/kg heating value of banana agri-residual, as obtained from equation 3 and 5.845 kW boiler capacity, the corresponding determined banana agri-residual consumption rate was 1.53 kg/h. This agrees with that obtained from the current study of 1.51 kg/h (i.e., 36.3 kg/ day).

Thermal energy storage was required to buffer the unstable heat generated by the bio-boiler to maintain the stability of the adsorption chiller operation. As shown in Figure 13, increasing the heat storage

volume increased the biomass required to generate the required heat at all boiler-setting temperatures. The reason behind that was the increase in heat storage losses as the heat storage size and boiler set temperature increased due to increasing the heat storage's surface area simultaneously with the difference between heat storage and ambient temperatures, as shown in Figure 13b. For example, at 95 °C, the increase in biomass consumption between heat storage 0.01 and 1 m^3 was 3 kg/day, while at 65 °C, the increase in the required biomass was 1.5 kg/day, due to the lower heat storage losses at 65 °C compared to that at 95 °C. However, the cooling system's performance was hardly affected by the increase in heat storage volume, in which the COP remained nearly unchanged throughout the range of heat storage size, as seen in Figure 13C. The same trends were observed at all boiler set temperatures. On the other hand, with regards to cold storage, it was observed that integrating cold storage with the bio-boiler and solar-powered cooling systems had little effect on the performance of both systems and the cold store temperature. As such, it was not included in the economic and environmental analysis.

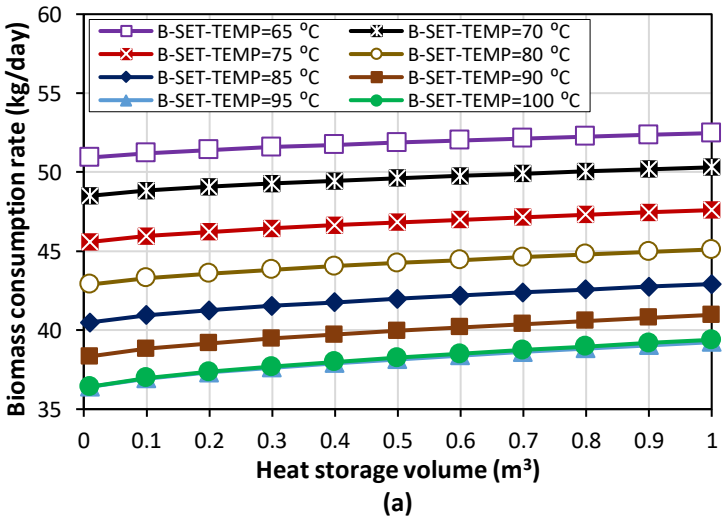

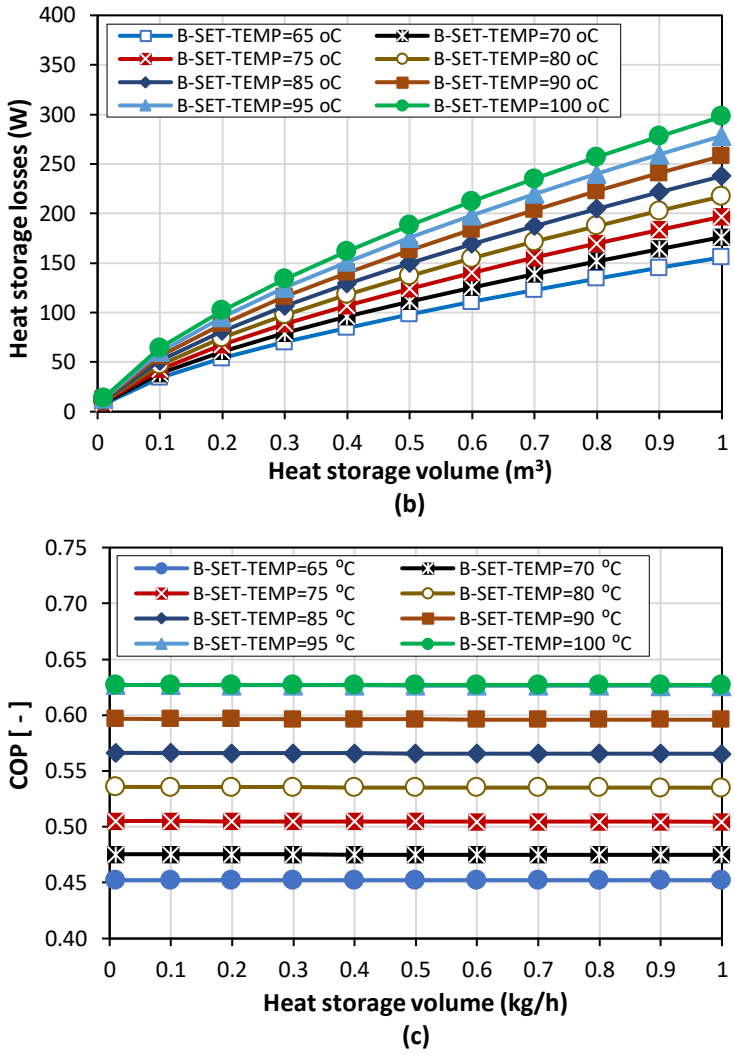

Figure 13. Effect of hot storage size on (a)-Biomass consumption rate (b)-Heat storage losses and (c)-COP (at set temperature 95 °C & hot water flow rate 601 kg/h)

Figure 14 shows the cold room temperature throughout the year at the optimal boiler's setting temperature of 95 °C, benchmarked against the operation at 65 °C. On the one hand, the boiler setting temperature of 65 °C cannot attain the cold room temperature of 10 °C throughout the year, even though the biomass combustion rate is high, primarily because of the poor energy conversion efficiency of the chiller. On the other hand, the optimisation study aimed to maintain the cold room at 10 °C and maximise the energy conversion efficiency, which yielded the optimal combination of 601.25 kg/h, 0.01 m^3 and 95.125 °C for biomass combustion rate, thermal energy storage size, and boiler setting temperature.

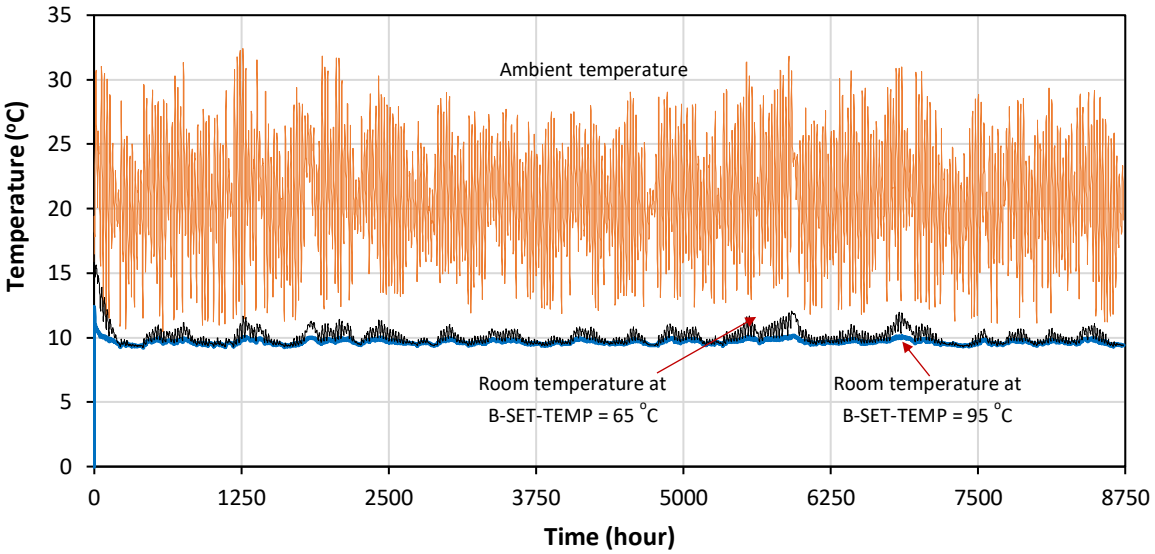

Figure 14. Hourly variation of room and ambient temperatures at optimal boiler setting temperatures 95 °C benchmarked against the temperature of 65 °C, and the hot water flow rate 601 kg/h and heat storage 0.01 m^3. The aimed cold room setting temperature is 10 °C.

Figure 15 shows the required boiler input and output energy, transferred to the chiller, and CO2 captured at different boiler-setting temperatures at constant boiler mass flow and heat storage volume. The required energies depend on the cooling system performance, which requires high energy at a low boiler set temperature due to low COP and vice versa. The CO_2 capture system consumed 20% of the boiler energy, whereas the remaining 80% was delivered to the hot storage to power the chiller. A small portion was lost from the hot storage to its surroundings, where heat loss increased as the boiler set temperature increased, as shown in Figure 16. A certain amount of boiler energy input was lost directly from the boiler to its surroundings through flue gases, as presented in Figure 16, where losses decreased as the boiler set temperature increased because of the decrease in the required boiler input energy resulting from the high COP at high heat temperature. The heat loss from the boiler is determined using equation 17. All required energies and boiler energy losses inversely followed the COP trend, where COP for silica gel/water adsorption chiller was barely affected beyond the heating source temperature of 100 °C [59].

$$Q_{loss} = Q_{boiler-input} - Q_{boiler-output} - Q_{exhaust} \quad (17)$$

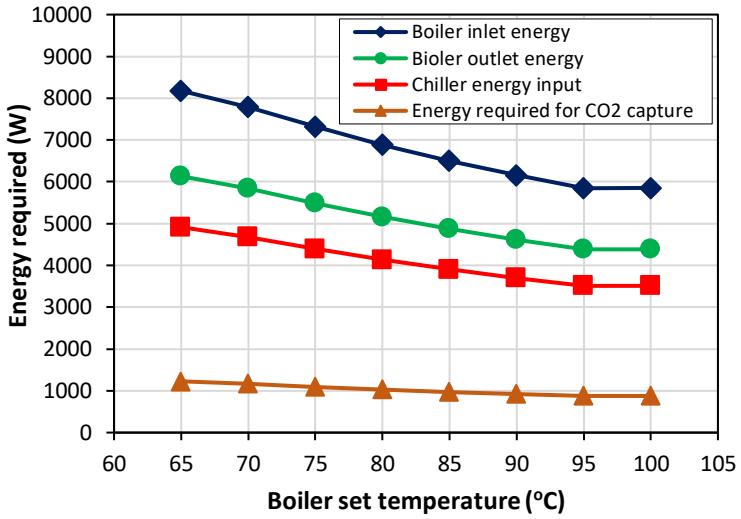

Figure 15. The system required energy, boiler input, output energy, chiller heat input, and CO_2 capture versus boiler setting temperature.

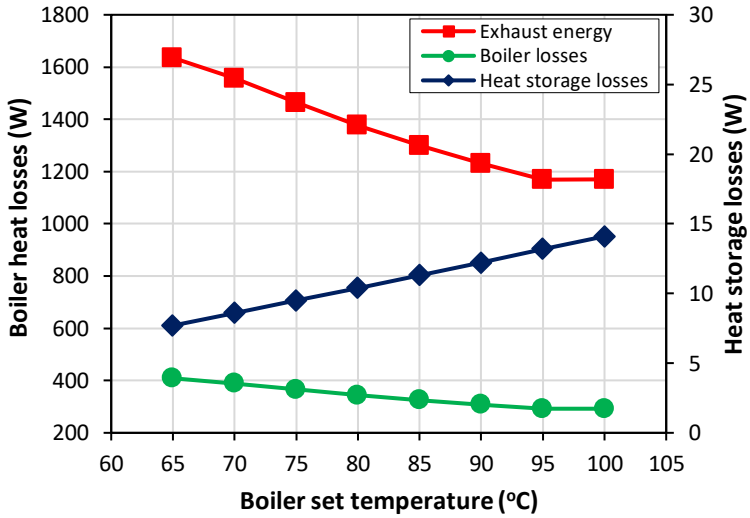

Figure 16. Boiler and hot storage energy losses versus boiler setting temperature.

3.3. Solar thermal-driven cooling system

The optimal solar ETC and heat storage were determined to achieve the maximum possible solar fraction. The solar fraction is the ratio between the amount of heat delivered from the solar collector and the amount of energy required to meet the cooling demand throughout the year. The solar fraction is strongly dependent on the overall energy conversion efficiency of the system, which combines the effect of the solar collector efficiency and the performance of the adsorption cooling system, as reported by Alammar et al. [60].

Figure 17 shows the solar fraction at different heat storage volumes and collector areas. It can be observed that the solar fraction increases as the combined collector area and heat storage volume

increases because of providing a sufficient grade and quantity of heat to maintain the operation of the adsorption chiller sufficiently efficient. On the other hand, low collector areas and large heat storage size combinations do not provide a good grade of heat to drive the adsorption chiller efficiently.

Using a collector area of 35 m^2 exhibited low solar fractions, ranging between 84% and 91% within the investigated range of heat storage size; as such, it did not meet the desired cold store setting temperature of 10 °C. For a collector area of 40 m^2, solar fractions of about 93% and 98% were obtained at storage volumes of 10 and 15 m^3. Finally, using a collector area of 45 m^2 achieved a solar fraction of nearly 100% at storage volumes of 10 and 15 m^3, whereas using 50 m^2 provided a solar fraction of 100% at 8, 10, and 15 m^3 storage sizes. In agreement with the literature, similar trends in the solar fraction were reported by Sokhansefat et al. and Román et al. [50], [61].

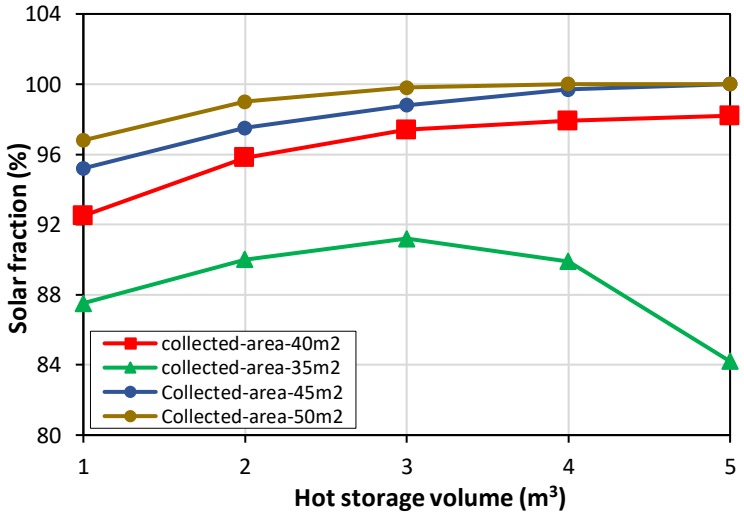

Figure 17. Thermal solar fraction versus hot storage size at different collector areas [60]

3.4. Electric power requirements for adsorption refrigeration systems

Electric energy is required to drive the auxiliary components, such as circulating pumps for heat transfer fluid (e.g., solar hot water loop, chiller hot water loop, and chiller heat sink loop), dry coolers' fans, and controllers in the integrated systems. The electric power required to operate the pumps and fans was 200 W, and for the adsorption chiller controllers and pumps was 150 W to maintain 24/7 operation, which counted for 5% of chiller cooling capacity (3 kW) according to the technical data sheet of Fahrenheit adsorption refrigeration unit used by Reda et al. [29]. The capacity of each PV module

simulated in the current study was 280 W, with an area of 1.6 m^2 per module (i.e., 175 W/m^2), as discussed in section 2.6.

Figure 18 presents the effect of the battery capacity on the solar fraction at different PV modules numbers. It was noticed that the solar fraction increased as the PV modules and battery storage capacity increased. The increase in solar fraction decreased as the PV modules' number, and battery storage capacity increased, mostly above 10 modules and 10 kWh. For example, using 6 PV modules showed a small solar fraction, and a negligible increase in the solar fraction was attained after a battery capacity of 10 kWh, which indicates that the power harnessed by 6 PV does not meet the system requirements. This was also the case when a 6 kWh battery capacity was coupled with all PV modules. It can also be observed that PV modules/battery capacity combinations of 10 modules / 20 kWh, 12 modules / 16 kWh, 14 modules / 14 kWh, and 16 modules / 12 kWh provided a solar fraction of nearly 100%, which can operate the system 24/7 throughout the year.

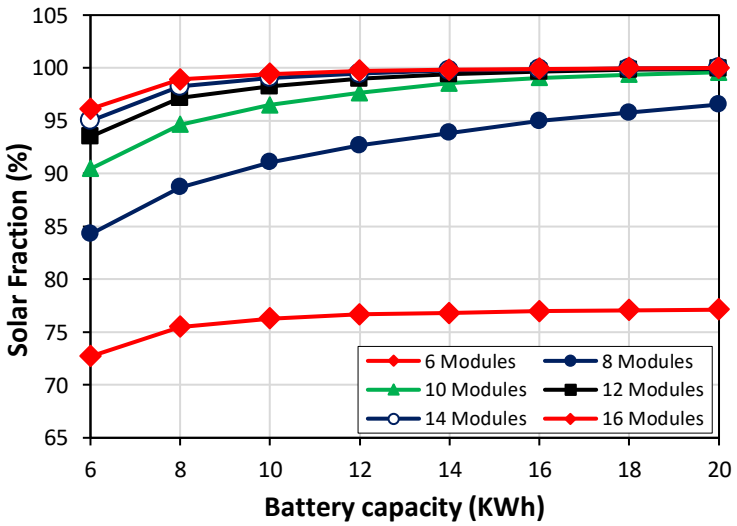

Figure 18. Variation of PV solar fraction with battery capacity at different PV modules number

3.5. Technical optimal parameters

The optimal alternatives for the solar and biomass systems and their required PV/battery subsystem are populated in Table 7. For the solar cooling system, although a combination of 45 m^2 collector area and 6 m^3 heat storage volume provided a solar fraction of 98%, it appeared to be more economically viable, which was elaborated on in the following sections. Although the solar fraction of 98% led to a 2%

deficit (equivalent to 48 minutes per day), it does not affect the cold room desired temperature of 10 °C, as the thermal inertia of the room and crops can maintain it shown in figure 14.

Table 7. Optimised systems' requirements

Solar thermal cooling system			PV system for pump & control		
Collector area, m^2	Storage size, m^3	Solar fraction (%)	PV modules number	Battery capacity kWh	Solar Fraction **(%)**
50	8	100	10	20	100
45	10	100	12	16	100
45	8	99	14	14	100
45	6	98	16	16	100
Biomass cooling system					
Boiler inlet energy, W	Boiler outlet Energy, W	Daily fuel rate, kg/day	Boiler set temp. $^{\circ}C$	Storage size, m^3	Flow rate kg/h
5845	4384	36.3	95.125	0.01	601.25

3.6. Economic feasibility and environmental impact

Part of assessing the integrated systems' feasibility is studying their economic and environmental impacts and benchmarking them against the conventional vapour compression cooling system driven by grid electricity. A simplified cost and environmental analysis, based on the subsystems' life cycle cost and environmental impact, were undertaken for three different durations of 15, 25, and 30 years. As listed in Table 8, 15 years is the lifespan of the battery and inverter and about double the lifetime of the electric chiller, 25 years includes the second lifetime of PV, ETC solar collectors, and 30 years is the double life of the battery and inverter.

3.6.1. Economic feasibility

Table 9 shows the specific cost for the main components. In this study, the dried and processed banana tree waste cost was initially considered the same price as the commercially available wood pellets biomass. Although banana agri-waste circulated directly at the farm level- additional pre-processing, logistics, and storage costs are anticipated to be lower, as the retail price of the wooden pellets includes additional manufacturing and retailing costs. Therefore, equating banana agri-waste and wood pellet prices as an initial benchmark can be acceptable. The cost of each component was considered linearly proportional to the size [54]. When the cost analysis duration exceeded a certain lifespan, an additional investment cost was added, proportional to the additional lifetime.

Building on the four technical optimal combinations of PV modules/battery storage capacities shown in Table 7, a sole combination of 12 PV modules / 16 kWh battery appeared to be more economically and environmentally viable. They showed the lowest cost (for 25 and 30 years lifetime) and GWP among the available alternatives. Considering the reduction of the required installation area, especially for the solar thermal system, which requires a relatively larger land area, an alternative combination of 12 modules / 16 kWh can provide the lowest cost and environmental impact.

Table 8. Components' lifetime (year)

Items	Lifetime
Adsorption chiller [62]	20
Electric chiller [63]	8
PV&ETC panels [63]	20
Battery [54]	15
Inverter [54]	15
Biomass boiler [64]	20

Table 9. Components cost

Items	cost	Units
Adsorption chiller [29]	1580	USD/kWc
Adsorption chiller maintenance [29]	1.58	USD/kWc/y
Electric chiller [54]	469	USD/kWc
Electric chiller maintenance [54]	10.78	USD/kWc/y
ETC panels [65]	330	USD/m^2
PV panels [46]	175	USD/module
PV operating [54]	7.39	USD/kWp/y
Heat storage [62]	600	USD/m^3
Battery [54]	380	USD/kWh
Battery operating [54]	11.3	USD/kWh/y
Inverter [66]	62	USD/kWh
Biomass boiler [8]	5500	USD/unit
Biomass fuel [67]	0.2	USD/kg
Pump [68]	$750*Wp^{0.4*}$	USD
Electricity tariff	0.31	USD/kWh

*Wp is the pump work in kW

Figure 18 compares the capital cost, including the replacement cost, and the operating cost of the solar, biomass, and electric chiller cooling systems for the investigated durations. For 15 years lifetime, it can be observed that the currently existing mechanical vapour compression system driven by the grid electricity exhibited the lowest cost compared to solar thermal and biomass-driven systems; 37564, 44096 and 70566 USD, respectively. However, the solar thermal-driven system presented the lowest cost compared to vapour compression and biomass systems; 58311, 62457 and 108723 USD for 25

years, and 69118, 74902 and 130333 USD for 30 years, respectively. Figure 19 shows that the difference in the cost for the three systems increased as the cost analysis duration increased because of the accumulated energy operating cost by the mechanical vapour compression cooling system (electricity cost), as well as the biomass system (fuel cost). The bioenergy cost increased at a higher rate (rise of 59767 USD from 15 to 30 years) than the electric energy (rise of 37338 USD from 15 to 30 years) due to higher operating cost represented by daily biomass consumption. However, the increase in the solar system's cost (rise of 25022 USD from 15 to 30 years) mainly resulted from the increase in the capital cost due the replacement of system components, and the highest shares arose from the replacement of the electric battery (two times), due to exceeding its lifespan after 15 years and the ETC panels and adsorption ciller after 20 years. For circulating banana agri-waste to be commercially competitive, the pre-processing, logistics, and storage cost should not exceed 0.05-0.07 USD per kg, as banana agri-waste is initially free of charge.

Compared to the other published work, Al-Ugla et al. [69] determined the power consumption of an electric chiller for different electricity tariffs. For 0.31 USD/kWh, the yearly cost of 10 hours/day during daytime only per $kW_{cooling}$ was 451 USD/year/$kW_{cooling}$. Considering the electric cooling system in the current study ran 24/7 year-round, which resulted in about 905 USD/year/kW; this is almost the same as the figure obtained in the current study of 909 USD/year/$kW_{cooling}$. For the solar thermal-driven cooling system, Reda et al. [29] reported a specific investment cost of about 5492 USD/$kW_{cooling}$ (4615 €/kW) for a 100% solar-driven adsorption refrigeration system, compared to about 10363 USD/$kW_{cooling}$ obtained in the present work, excluding the investment cost of the PV solar system. The higher specific investment cost obtained in the present work can be attributed mainly to the adopted higher solar collector and heat storage costs compared to the values used in [29]. Besides, the cost of the adsorption refrigeration unit was considered for a capacity of 8 kW, the smallest commercially available capacity, while the current system capacity is only 3 kW.

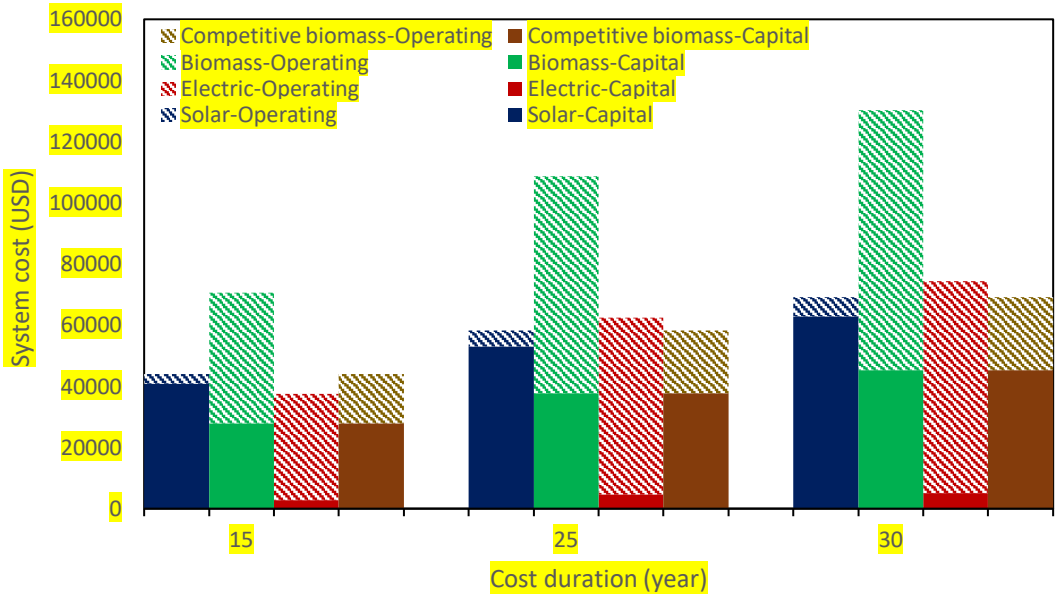

Figure 19. Variation of cost with the number of years for three different cooling systems

3.6.1. Environmental impact

The CO_2 emission for the three systems was determined based on 25 years and the CO_2 emission factors illustrated in Table 10. The CO_2 emissions for the solar cooling system included ETC, heat storage, PV panels, inverters, and electric batteries. It is noteworthy mentioning that the emission factor for PV, batteries, and inverter represents the emission during their lifespan, including material production, manufacturing, transportation, and recycling. For the mechanical vapour compression system driven by the grid electricity, the CO_2 emission resulted from the electricity generation and the CO_2 equivalent to the global warming index of the refrigerant. For the biomass-driven system, the CO_2 emission by the combustion of banana agri-waste, PV panels, inverter, and battery storage during their life cycle was considered. For banana biomass combustion, proposing oxyfuel carbon capture technique reduced CO_2 emitted from bio-boiler by nearly 90% [24], so only 10% of the CO_2 emission factor was considered.

The GWP for the utilised refrigerant (R410A) assumed that the refrigerant charge was 1kg, according to the refrigeration system capacity and considering two system replacements during the 25 years life cycle [63]. The refrigerant's leakage during the lifetime of the vapour compression system was omitted.

Table 10. CO_2 emission calculation

Items	Emission factor $kgCO_2e/kWh$	CO_2 footprint calculations for 25 years
ETC& heat storage	0.0222 [70]*	ETC Energy output/year×0.0222×25 years
PV& inverter	0.0443 [70]	PV power output/year×0.0443×25 years
Electric battery	173 [71]	Battery capacity in kWh×173×2 (one replacement)
R410A	$2088/kg_{refrigerant}$ [72]	1kg refrigerant×2088×3 (two replacements)
Electricity (Rwanda)	0.390 [73]	Electric power consumption/year×0.39×25 years
Banana waste	$0.2034/kWh_{th}$ [74]**	bio-boiler input energy/year×0.2034×10%×25 years

*the values for the ETC and heat storage was per m^2 in the reference and adaption was made to convert them in kWh in this study.
**using equation (12) in this reference to calculate CO_2 emission factor for banana waste

Table 11 presents the equivalent total CO_2 emission for the three systems. It can be observed that the solar cooling system produced nearly 75% less CO_2 emission than the analogous mechanical vapour compression system driven by the grid electricity; it also generated about 47% less CO_2 than the biomass cooling system. 92% of the CO_2 emission of the mechanical vapour compression refrigeration system was generated from the electric energy consumed, due to its high CO_2 emission factor of 0.39 kgCO2e/kWh, whereas 8% represented the GWP of the utilised refrigerant, as shown in Figure 20. In the biomass-driven refrigeration system, biomass combustion released 70% of the CO_2, whereas the PV arrays and batteries counted for 16% and 14%, respectively. ETC & heat storage, PV panels, inverters, and batteries counted for 39%, 33%, and 28% of the system's CO2 emission for the solar thermal system. The amount of CO_2 emitted from the battery included one replacement after 15 years, whereas it represented three refrigerant's timespans, as the lifetime of the electric cooling machine is 8 years.

Table 11. CO_2 emission and cost for 25 year

System	ton CO_2e/25 years	USD Cost/25years
Solar cooling system+ PV system	20.1	58311
Biomass cooling system +PV system	38.2	108723
Electric chiller	77.8	62457

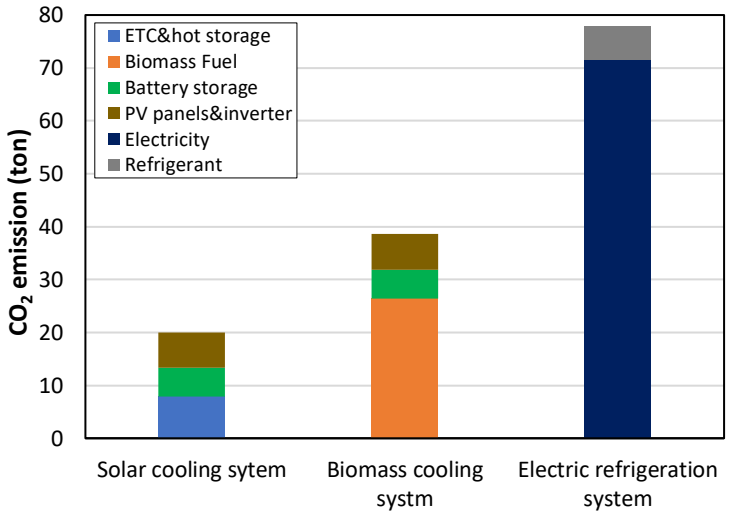

Figure 20. Amount of CO_2 emission for the three systems for 25 years

Although the current analysis at the integrated system level revealed that solar-driven cooling systems have the least GWP and cost among the investigated systems (least cost for 25 and 30 years lifetime), it is environmentally competitive when considering the carbon neutrality of bioenergy [8]. This is because the plant can absorb the same quantity of CO2 emitted during the processing of the plant-based biomass during its growth.

4. Conclusions and prospects

4.1. Conclusions

This paper aimed to study the technical, economic, and environmental feasibility of a novel sustainable standalone thermal-driven cooling package driven by biomass to address the lack of food cold chain in SSA countries, where Rwanda was used as a case study. As such, the proposed system was simulated and technically optimised to meet the end-users year-round 24/7 cooling demand. Furthermore, the optimised system was benchmarked against adsorption solar-driven and vapour compression refrigeration systems.

By utilising banana agri-waste as a feedstock for the bio-boiler for the bio-driven cooling system, the minimal biomass consumption of 36 kg/day, minimum boiler inlet energy of 5845 W, and maximum cooling performance of 0.62 was obtained at the optimal heat storage volume, heating water flow rates and boiler setting temperatures to 0.01 m^3, 601.25 kg/h and 95.125 °C. The energy conversion efficiency of the adsorption refrigeration system played a crucial role in optimising the integrated system, as some

lower heating temperatures (e.g., 65 ^{o}C), which demand higher biomass combustion rate, did not enable meeting the cooling demand at the cold room end. In a solar-driven adsorption cooling system, although the collector area of 45 m^2 combined with the storage volume of 6 m^3 provided a solar fraction of 98%, it stood to be the optimal integration after considering the life cycle economic benefits and environmental impacts. For both systems, 12 PV modules integrated with a 16 kWh battery satisfied the electric energy demanded by the systems' auxiliaries at minimal environmental impact and maximum economic benefits.

While the economic feasibility of bio-driven cooling at the integrated system level did not stand out compared to solar-driven adsorption and mechanical driven vapour compression refrigeration systems, it is viable if the pre-processing, logistics and storage cost of banana agri-waste was brought down to 0.07 USD for the investigated case study. Given that bioenergy is considered carbon-neutral at the broader levels, the bio-driven adsorption refrigeration system has competitive environmental merit after considering flue gas cleaning.

4.1. Prospects

Future work will be centred around using various sustainable working pairs at the adsorption refrigeration subsystem level to achieve lower temperatures and open opportunities for storing more comprehensive ranges of farm products (e.g., activated carbon/ methanol or ethanol) and integrating solar and biomass subsystems to achieve more viable integrated systems. Besides, there is a potential to investigate a broader range of techno-economic-ecological viable cooling packages. The exergy analysis will be at the centre of future work to quantify the lost opportunities for energy harvesting and utilisation to enhance the integrated systems toward providing a more efficient energy conversion.

Acknowledgement

Research England, UK funded this work.

REFERENCES

[1] Food and Agriculture Organization, "Food wastage footprint Impacts on natural resources," 2013. [Online]. Available: www.fao.org/publications.

[2] T. . Bond, M., Meacham, T., Bhunnoo, R. and Benton, "Food waste within global food systems," 2013. [Online]. Available: A Global Food Security report (www.foodsecurity.ac.uk).

[3] M. Sheahan and C. B. Barrett, "Review : Food loss and waste in Sub-Saharan Africa," *Food Policy*, vol. 70, pp. 1–12, 2017, doi: 10.1016/j.foodpol.2017.03.012.

[4] Food and Agriculture Organisation, "The State of Food and Acriculture: Moving Forward on Food Loss and Waste Reduction," 2019.

[5] Food and Agriculture Organization, "Agroindustry Policy Brief: Developing the cold chain in the agrifood sector in sub-Saharan Africa," 2016.

[6] Rwandan Ministry of Infrastructure, "Republic of Rwanda, National Energy Policy and Strategy 2008-2012," 2009.

[7] Rwanda Utilities Regulatory Authority, "Press release for Electricity Tariffs." 2020.

[8] R. . Gorissen, "Wood pellets and renewable biomass based heating," 2017.

[9] A. G. Olabi, "Circular economy and renewable energy," *Energy*, vol. 181, pp. 450–454, 2019, doi: 10.1016/j.energy.2019.05.196.

[10] H. Jouhara and A. G. Olabi, "Editorial: Industrial waste heat recovery," *Energy*, vol. 160, pp. 1–2, 2018, doi: 10.1016/j.energy.2018.07.013.

[11] National Institute of Statistics of Rwanda (NISR), "Seasonal Agricultural Survey," Kigali, 2016.

[12] E. R. K. Fernandes, C. Marangoni, O. Souza, and N. Sellin, "Thermochemical characterisation of banana leaves as a potential energy source," *Energy Convers. Manag.*, vol. 75, pp. 603–608, 2013, doi: 10.1016/j.enconman.2013.08.008.

[13] I. Kabenge, G. Omulo, N. Banadda, J. Seay, A. Zziwa, and N. Kiggundu, "Characterisation of Banana Peels Wastes as Potential Slow Pyrolysis Feedstock," *J. Sustain. Dev.*, vol. 11, no. 2, p. 14, 2018, doi: 10.5539/jsd.v11n2p14.

[14] K. Ku Ahmad, K. Sazali, and A. A. Kamarolzaman, "Characterisation of fuel briquettes from banana tree waste," *Mater. Today Proc.*, vol. 5, no. 10, pp. 21744–21752, 2018, doi: 10.1016/j.matpr.2018.07.027.

[15] N. Abdullah, F. Sulaiman, and R. M. Taib, "Characterisation of banana (Musa spp.) plantation

wastes as a potential renewable energy source," *AIP Conf. Proc.*, vol. 1528, no. August, pp. 325–330, 2013, doi: 10.1063/1.4803618.

[16] W. P. Clarke, P. Radnidge, T. E. Lai, P. D. Jensen, and M. T. Hardin, "Digestion of waste bananas to generate energy in Australia," *Waste Manag.*, vol. 28, no. 3, pp. 527–533, 2008, doi: 10.1016/j.wasman.2007.01.012.

[17] N. Pisutpaisal, S. Boonyawanich, and H. Saowaluck, "Feasibility of biomethane production from banana peel," *Energy Procedia*, vol. 50, pp. 782–788, 2014, doi: 10.1016/j.egypro.2014.06.096.

[18] S. Achinas, J. Krooneman, and G. J. W. Euverink, "Enhanced Biogas Production from the Anaerobic Batch Treatment of Banana Peels," *Engineering*, vol. 5, no. 5, pp. 970–978, 2019, doi: 10.1016/j.eng.2018.11.036.

[19] V. C. Kalia, V. Sonakya, and N. Raizada, "Anaerobic digestion of banana stem waste," *Bioresour. Technol.*, vol. 73, no. 2, pp. 191–193, 2000, doi: 10.1016/S0960-8524(99)00172-8.

[20] S. Bhushan, M. S. Rana, Mamta, N. Nandan, and S. K. Prajapati, "Energy harnessing from banana plant wastes: A review," *Bioresour. Technol. Reports*, vol. 7, no. March, p. 100212, 2019, doi: 10.1016/j.biteb.2019.100212.

[21] A. Nurdiawati, A. Mosqueda, B. Lokahita, and K. Yoshikawa, "Tapping Indonesia ' s bioenergy potential : Solid biofuel production from banana leaves by employing hydrothermal treatment," *doi 10.17605/OSF.IO/US2EC*, [Online]. Available: doi: 10.17605/OSF.IO/US2EC.

[22] Z. Zhang, T. N. Borhani, and A. G. Olabi, "Status and perspective of CO2 absorption process," *Energy*, vol. 205, p. 118057, 2020, doi: 10.1016/j.energy.2020.118057.

[23] F. Sher, M. A. Pans, C. Sun, C. Snape, and H. Liu, "Oxy-fuel combustion study of biomass fuels in a 20 kWth fluidised bed combustor," *Fuel*, vol. 215, no. November 2017, pp. 778–786, 2018, doi: 10.1016/j.fuel.2017.11.039.

[24] T. Uchida, T. Goto, T. Yamada, T. Kiga, and C. Spero, "Oxyfuel combustion as CO2 capture technology advancing for practical use - Callide oxyfuel project," *Energy Procedia*, vol. 37, pp. 1471–1479, 2013, doi: 10.1016/j.egypro.2013.06.022.

[25] R. AL-Dadah, S. Mahmoud, E. Elsayed, P. Youssef, and F. Al-Mousawi, "Metal-organic framework materials for adsorption heat pumps," *Energy*, vol. 190, p. 116356, 2020, doi: 10.1016/j.energy.2019.116356.

[26] M. Mikhaeil, M. Gaderer, and B. Dawoud, "On the development of an innovative adsorber plate heat exchanger for adsorption heat transformation processes ; an experimental and numerical

study," *Energy*, vol. 207, p. 118272, 2020, doi: 10.1016/j.energy.2020.118272.

[27] C. Monné, S. Alonso, F. Palacín, and L. Serra, "Monitoring and simulation of an existing solar powered absorption cooling system in Zaragoza (Spain)," *Appl. Therm. Eng.*, vol. 31, no. 1, pp. 28–35, 2011, doi: 10.1016/j.applthermaleng.2010.08.002.

[28] L. F. Sim, "Numerical modelling of a solar thermal cooling system under arid weather conditions," *Renew. Energy*, vol. 67, pp. 186–191, 2014, doi: 10.1016/j.renene.2013.11.032.

[29] A. M. Reda, A. H. H. Ali, M. G. Morsy, and I. S. Taha, "Design optimisation of a residential scale solar driven adsorption cooling system in upper Egypt based," *Energy Build.*, vol. 130, no. October, pp. 843–856, 2016, doi: 10.1016/j.enbuild.2016.09.011.

[30] A. Zimakov, "Bioenergy in EU: Problems and Prospects," *Mirovaya Ekon. i mezhdunarodnye Otnos.*, vol. 64, no. 8, pp. 81–90, 2020.

[31] P. Iodice and M. Cardone, "Impact of a trigeneration power system fuelled by vegetable oil on environmental air pollution by numerical simulations," 2020, doi: 10.1177/0958305X19888879.

[32] M. Villa-arrieta and A. Sumper, "A model for an economic evaluation of energy systems using TRNSYS," *Appl. Energy*, vol. 215, no. February, pp. 765–777, 2018, doi: 10.1016/j.apenergy.2018.02.045.

[33] TRNSYS 18, "Standard components library," TRANSSOLAR Energietechnik GmbH, 2017.

[34] TRNSYS 18, "Multizone Building modeling with Type56 and TRNBuild Solar," TRANSSOLAR Energietechnik GmbH, 2017.

[35] The American Society of Heating Refrigerating and Air-Conditioning, Ed., "Commodity storage requirements," in *ASHRAE Handbook—Refrigeration*, 2018, p. 10.

[36] B. R. Paranjpey, "Potato Cold Storage Load Calculations per NHB Standard 01 : 2010," *Cold Chain*, no. December, 2014.

[37] N. G. Faith *et al.*, "ASHRAE Handbook-Refrigeration (SI)-THERMAL PROPERTIES OF FOODS," in *Growth (Lakeland)*, vol. 66, no. 5, 2018, pp. 918–26.

[38] M. Y. Haller *et al.*, "A unified model for the simulation of oil, gas and biomass space heating boilers for energy estimating purposes. Part I: Model development," 2011.

[39] S. Restrepo-valencia and A. Walter, "Techno-Economic Assessment of Bio-Energy in a Typical Sugarcane Mill in Brazil," *Energies*, 2019, doi: 10.3390/en12061129.

[40] K. Andersson and F. Johnsson, "Process evaluation of an 865 MW e lignite fired O 2 / CO 2 power plant," *Energy Convers. Manag.*, vol. 47, pp. 3487–3498, 2006, doi:

10.1016/j.enconman.2005.10.017.

[41] S. M. Mousavian and M. T. Mansouri, “Conceptual feasibility study of retrofitting coal-fired power plant with oxyfuel combustion,” *Proc. Inst. Mech. Eng. Part A J. Power Energy*, vol. 225, no. x, pp. 689–700, 2011, doi: 10.1177/0957650911406480.

[42] M. B. Toftegaard, J. Brix, P. A. Jensen, P. Glarborg, and A. D. Jensen, “Oxy-fuel combustion of solid fuels,” *Prog. Energy Combust. Sci.*, vol. 36, no. 5, pp. 581–625, 2010, doi: 10.1016/j.pecs.2010.02.001.

[43] M. S. A. Khan, A. W. Badar, T. Talha, M. W. Khan, and F. S. Butt, “Configuration based modeling and performance analysis of single effect solar absorption cooling system in TRNSYS,” *Energy Convers. Manag.*, vol. 157, no. December 2017, pp. 351–363, 2018, doi: 10.1016/j.enconman.2017.12.024.

[44] L. Thermal Energy System Specialists, *HVAC Library Mathematical Reference*, vol. 06. Wisconsin, USA.

[45] A. G. Olabi, C. Onumaegbu, T. Wilberforce, M. Ramadan, M. A. Abdelkareem, and A. H. Al – Alami, “Critical review of energy storage systems,” *Energy*, vol. 214, p. 118987, 2021, doi: 10.1016/j.energy.2020.118987.

[46] Solar supplier UK, “Photovoltaic PV (solar panels).” https://solarsuppliesuk.co.uk/product-category/solar-pv/solar-panels/.

[47] X. Wang and M. Dennis, “A comparison of battery and phase change coolth storage in a PV cooling system under different climates,” *Sustain. Cities Soc.*, vol. 36, no. October 2017, pp. 92–98, 2018, doi: 10.1016/j.scs.2017.09.035.

[48] A. Esfandyari, A. Świerc, B. Norton, M. Conlon, and S. J. Mccormack, “Modelling and Energy Management Optimisation of Battery Energy Storage System (BESS) Based Photovoltaic Charging Station (PV-CS) for University Campus,” no. Swc, p. 2015, 2015.

[49] TRNSYS 18, “Using the Simulation Studio.” TRANSSOLAR Energietechnik GmbH, 2017.

[50] T. Sokhansefat, D. Mohammadi, A. Kasaeian, and A. R. Mahmoudi, “Simulation and parametric study of a 5-ton solar absorption cooling system in Tehran,” *Energy Convers. Manag.*, vol. 148, pp. 339–351, 2017, doi: 10.1016/j.enconman.2017.05.070.

[51] T. He, X. Zhang, C. Wang, M. Wang, B. Li, and N. Xue, “Application of solar thermal cooling system driven by low temperature heat source in China,” *Energy Procedia*, vol. 70, pp. 454–461, 2015, doi: 10.1016/j.egypro.2015.02.147.

[52] P. J. Martınez, C. Martınez, and M. Lucas, “Design and test results of a low-capacity solar

cooling system in Alicante (Spain),” *Sol. Energy*, vol. 86, pp. 2950–2960, 2012, doi: 10.1016/j.solener.2012.06.030.

[53] U. Eicker, D. Pietruschka, and R. Pesch, “Heat rejection and primary energy efficiency of solar driven absorption cooling systems,” *Int. J. Refrig.*, vol. 35, no. 3, pp. 729–738, 2012, doi: 10.1016/j.ijrefrig.2012.01.012.

[54] C. Luerssen, O. Gandhi, T. Reindl, C. Sekhar, and D. Cheong, “Life cycle cost analysis (LCCA) of PV-powered cooling systems with thermal energy and battery storage for off-grid applications,” *Appl. Energy*, vol. 273, no. May, p. 115145, 2020, doi: 10.1016/j.apenergy.2020.115145.

[55] D. Firmanda, A. Riza, S. I. H. Gilani, and M. S. Aris, “Measurement and simulation of a standalone photovoltaic system for residential lighting in Malaysia,” in *International Symposium on Environment Friendly Energies in Electrical Applications*, 2011, vol. 2, no. 1.

[56] A. R. M. Rezk and R. K. Al-dadah, “Physical and operating conditions effects on silica gel / water adsorption chiller performance,” *Appl. Energy*, vol. 89, no. 1, pp. 142–149, 2012, doi: 10.1016/j.apenergy.2010.11.021.

[57] F. He, K. Nagano, and J. Togawa, “Experimental study and development of a low-cost 1 kW adsorption chiller using composite adsorbent based on natural mesoporous material,” *Energy*, vol. 209, p. 118365, 2020, doi: 10.1016/j.energy.2020.118365.

[58] K. M. Almohammadi and K. Harby, “Operational conditions optimisation of a proposed solar-powered adsorption cooling system : Experimental , modeling , and optimisation algorithm techniques,” *Energy*, vol. 206, p. 118007, 2020, doi: 10.1016/j.energy.2020.118007.

[59] M. Noro and R. M. Lazzarin, “Solar cooling between thermal and photovoltaic: An energy and economic comparative study in the Mediterranean conditions,” *Energy*, vol. 73, pp. 453–464, 2014, doi: 10.1016/j.energy.2014.06.035.

[60] A. A. Alammar, A. Rezk, A. Alaswad, S. Decker, J. Ruhumuliza, and G. Q. Gasana, “Modelling of cold store for agro-products using solar-driven adsorption chiller under Rwandan environmental conditions,” in *ENERGY PROCEEDINGS, International Conference on Applied Energy*, 2020, pp. 1–5.

[61] J. C. Román, R. J. R. Domínguez, A. R. Martínez, and S. P. Pedro, “Thermal Analysis of an Absorption and Adsorption Cooling Chillers Using a Modulating Temperature Valve,” IntechOpen, pp. 0–15.

[62] A. Alahmer, X. Wang, and K. C. A. Alam, “Dynamic and Economic Investigation of a Solar

Thermal-Driven Two-Bed Adsorption Chiller under Perth Climatic Conditions," *Energies*, 2020.

[63] U. Eicker, A. Colmenar-Santos, L. Teran, M. Cotrado, and D. Borge-Diez, "Economic evaluation of solar thermal and photovoltaic cooling systems through simulation in different climatic conditions: An analysis in three different cities in Europe," *Energy Build.*, vol. 70, pp. 207–223, 2014, doi: 10.1016/j.enbuild.2013.11.061.

[64] EDEN, "Biomass Boilers." https://www.edensustainable.co.uk/domestic/domestic-info/.

[65] Navitron UK, "Solar Keymarked Evacuated Tube Solar Panel." https://www.navitron.org.uk/sfb-al-slimline-30-tube-58mm-solar-panel.

[66] M. Alobaid, B. Hughes, J. K. Calautit, D. O'Connor, and A. Heyes, "A review of solar driven absorption cooling with photovoltaic thermal systems," *Renew. Sustain. Energy Rev.*, vol. 76, no. February, pp. 728–742, 2017, doi: 10.1016/j.rser.2017.03.081.

[67] P. Jagger and I. Das, "Energy for Sustainable Development Implementation and scale-up of a biomass pellet and improved cookstove enterprise in Rwanda," *Energy Sustain. Dev.*, vol. 46, pp. 32–41, 2018, doi: 10.1016/j.esd.2018.06.005.

[68] B. H. Gebreslassie, G. Guillén-gosálbez, L. Jiménez, and D. Boer, "Design of environmentally conscious absorption cooling systems via multi-objective optimisation and life cycle assessment," *Appl. Energy*, vol. 86, no. 9, pp. 1712–1722, 2009, doi: 10.1016/j.apenergy.2008.11.019.

[69] A. A. Al-ugla and S. A. M. Said, "Techno-economic analysis of solar-assisted air-conditioning systems for commercial buildings in Saudi Arabia," *Renew. Sustain. Energy Rev.*, vol. 54, pp. 1301–1310, 2016, doi: 10.1016/j.rser.2015.10.047.

[70] M. Milousi, M. Souliotis, G. Arampatzis, and S. Papaefthimiou, "Evaluating the environmental performance of solar energy systems through a combined life cycle assessment and cost analysis," *Sustain.*, vol. 11, no. 9, 2019, doi: 10.3390/su11092539.

[71] C. Spanos, D. E. Turney, and V. Fthenakis, "Life-cycle analysis of fl ow-assisted nickel zinc- , manganese dioxide- , and valve-regulated lead-acid batteries designed for demand-charge reduction," *Renew. Sustain. Energy Rev.*, vol. 43, pp. 478–494, 2015, doi: 10.1016/j.rser.2014.10.072.

[72] Air Conditioning and Refrigration Industry Board, "2014 F-Gas Regulation and GWP Values," UK, 2015.

[73] A. Gouldson, S. Colenbrander, A. Sudmant, N. Chilundika, and L. de Melo, "The Economics of

Low Carbon Cities, Kigali, Rwanda," University of Leeds, 2018.

[74] G. Maj, "Emission Factors and Energy Properties of Agro and Forest Biomass in Aspect of Sustainability of," *Energies*, 2018, doi: 10.3390/en11061516.